NUMERICAL STUDY ON THE PERFORMANCE OF SOLAR CHIMNEY POWER PLANT UNDER VARYING CHIMNEY DIVERGENCE ANGLE AND SOLAR RADIATION CONDITIONS

MAISARH TAREQ ABDULHAMEED AL-RAWE

FEBRUARY 2020

NUMERICAL STUDY ON THE PERFORMANCE OF SOLAR CHIMNEY POWER PLANT UNDER VARYING CHIMNEY DIVERGENCE ANGLE AND SOLAR RADIATION CONDITIONS

A THESIS SUBMITTED TO THE GRADUATE SCHOOL OF NATURAL AND APPLIED SCIENCES OF CANKAYA UNIVERSITY

BY

MAISARH TAREQ ABDULHAMEED AL-RAWE

IN PARTIAL FULFILLMENT OF THE REQUIREMENTS FOR
THE DEGREE OF MASTER OF SCIENCE IN
MECHANICAL ENGINEERING

FEBRUARY 2020

Approval of the Thesis: **Numerical Study on the Performance of Solar Chimney Power Plant under Varying Chimney Divergence Angle and Solar Radiation Conditions.**

Submitted by: **Maisarh Tareq Abdulhameed AL-RAWE**

Approval of the Graduate School of Natural and Applied Sciences, Çankaya University.

Prof. Dr.Can ÇOĞUN
Director

I certify that this thesis satisfies all the requirements as a thesis for the degree of Master of Science.

Prof. Dr. Haşmet TÜRKOĞLU
Head of Department

This is to certify that we have read this thesis and that in our opinion it is fully adequate, in scope and quality, as a thesis for the degree of Master of Science.

Assist. Prof. Dr. Ülkü Ece AYLI İNCE
Supervisor

Assist. Prof. Dr. Ekin ÖZGİRGİN YAPICI
Co-Supervisor

Examination Date: 04 / 02 / 2020

Examining Committee Members:

Prof. Dr. Haşmet TÜRKOĞLU	Çankaya Univ.
Assist. Prof. Dr. Özgür BAYER	Orta Doğu Teknik Univ.
Assist. Prof. Dr. Ülkü Ece AYLI İNCE	Çankaya Univ.

STATEMENT OF NON-PLAGIARISM PAGE

I hereby declare that all information in this document has been obtained and presented in accordance with academic rules and ethical conduct. I also declare that, as required by these rules and conduct, I have fully cited and referenced all material and results that are not original to this work.

Name, Last name: MAISARH TAREQ ABDULHAMEED AL-RAWE

Signature : 

Date : 04 / 02 / 2020

ABSTRACT

NUMERICAL STUDY ON THE PERFORMANCE OF SOLAR CHIMNEY POWER PLANT UNDER VARYING CHIMNEY DIVERGENCE ANGLE AND SOLAR RADIATION CONDITIONS

MAISARH TAREQ ABDULHAMEED AL-RAWE
M.Sc., Department of Mechanical Engineering

Supervisor: Assist. Prof. Dr. Ülkü Ece Ayli İnce
Co-Supervisor: Assist. Prof. Dr. Ekin Özgirgin Yapıcı

FEBRUARY 2020, 83 Pages

The solar chimney power plant is considered to be an important utilizations of solar energy because it is not expensive, simple to maintain and is available everywhere in the long term. The solar chimney power plant consists of three major components: the chimney, turbine and solar collector. The collector absorbs the irradiance and heats the air inside the system and a buoyancy force is created according to the different densities between the ambient cold air and the hot air inside the system and air flows upward in the chimney this air flow rise a turbine and thus power is generated. In this thesis, the effect of chimney geometry on SCPP performance is investigated. It was observed that the divergent chimney is the best. Therefore, the first part of this research studies on the impact of the divergence angle on performance. According to the results, up to a critical divergence angle, the output power increase with an increasing divergence angle. the inclination angle at 3^{o} is 2.18 times the benchmark case. In sight of the results, the best dimensions found for the model consist of a divergent chimney

height of 3.5 m, an inlet diameter of 25 cm, an outlet diameter of 61.68 cm, a collector diameter of 4 m and a height 6 cm. In the second part of this research, after determining the best model, analyses were carried out with different solar radiation and ambient temperatures for Ankara, Turkey at latitude 40° N and longitude 32.8° E. Ankara is characterized by cold winters with a low of daylight hours, and weather solar radiation. In contrast, in summer has high solar radiation compared to the other seasons with daylight hours of up to 13 hours. The spring and fall have moderate weather and medium amounts of irradiance. MATLAB code was developed to calculate the amount of solar radiation for different time of a day. Ambient temperature values were obtained from the State Meteorological Service. ANSYS Fluent was used to obtain power values for four different days (17 January, 15 April, 17 July and 15 October). According to the results, power output of the system is dependent on the solar radiation as well as the ambient temperature.

Keywords: Solar Energy, Daily Analysis, CFD, Divergent Chimney Power Plant, Numerical Simulation, SCPP

ÖZ

GÜNEŞ BACASI SANTRALİNDE BACA GENİŞLEME AÇISININ VE SOLAR RADYASYONUN PERFORMANSA ETKİSİNİN NÜMERİK OLARAK MODELLENMESİ

MAISARH TAREQ ABDULHAMEED AL-RAWE

Yüksek Lisans, Makine Mühendisliği Anabilim Dalı

Danışman: Dr. Öğr. Üyesi Ülkü Ece Ayli İnce
Eş-Danışman Dr. Öğr. Üyesi. Ekin Özgirgin Yapıcı

ŞUBAT 2020, 83 SAYFA

Güneş bacası solar enerjiden faydalanarak enerji üreten basit, maliyetsiz ve yenilenebilir bir kaynaktır. Güneş bacaları baca, kollektor ve türbin olmak üzere üç temel bileşenden oluşmaktadır. Kollektör radyasyon emilimi yapmakta ve system içerisindeki havanın ısınrarak yükselmesini sağlamaktadır. Varolan yoğunluk farkı sebebi ile kaldırma kuvveti meydana gelmekte ve bu kuvvet yardımı ile türbin dönerek hava yükselmektedir. Çalışma grubumuz ilk olarak güneş bacası geometrik parametrelerinin etkisini ve bacanın geoemtrik konfigürasyonunun performance olan etkilerini irdelemiştir. Elde edilen sonuçlara göre ıraksak baca en iyi performansı sağlamaktadır. Bu çalışmada ilk olarak ıraksama açısının performansa olan etkisi irdelenmiştir. Elde edilen sonuçlara göre kritik bir eğim açısına kadar güç artış göstermiştir. 3º eğimli ıraksak baca, baz duruma göre 2.18 kat daha fazla güç üretmektedir. Çalışma sonucunda gücü maksimize eden durum 3.5m baca yüksekliği, 25 cm giriş çapı, 61.68 cm çıkış çağı, 4m kollektör çapı ve 6 cm kollektör uzunluğunda elde edilmiştir.

Çalışmanın ikinci kısmında,solar radyasyonun ve ortam sıcaklığının Ankara, Türkiye için günlük incelemesi yapılmıştır. Kış aylarında solar radyasyon düşük iken yaz aylarında artış göstermekte ilkbahar ve sonbaharda ortalama bir radyasyon etkisi altında kalmaktadır. Yazın 13 saat civarında gün ışığına maruz kalmakta olan şehirde güneş bacasının kullanımının verimliliği araştırılmıştır.Saate göre dış hava koşullarına göre radyasyon hesaplaması geliştirilen MATLAB kodu ile yapılmıştır. Her bir sezondan bir gün seçilerek HAD analizleri ANSYS Fluent programı kullanılarak gerçekleştirilmiş ve sezonlara bağlı güç hesaplaması yapılmıştır. Sonuçlara göre, güç hava koşulları ve solar radyasyonun fonksiyonudur.

Anahtar Kelimeler: Solar Enerji, Günlük Analiz, Iraksak Güneş Bacası, HAD.

ACKNOWLEDGEMENTS

First of all, I thank my God Allah about everything. I would like to express my deep gratitude to my supervisor: Dr. Ülkü Ece AYLI İNCE and my Co-Supervisor Dr. Ekin ÖZGIRGIN YAPICI, for their guidance, enthusiastic encouragement and useful critiques of this research work.

I would like to thank the head of the mechanical engineering department Prof. Dr.Haşmet TÜRKOĞLU.

I would like to express my special appreciation and gratefulness to my father, my mother, my brothers and my sister for their support and encouragement to me during my study.

Special thanks to persons who helped me forget the trouble and tiredness, my dear wife's, my daughter Teba, my son Qasim.

I would like to thank my best friend who always stands me Osama AL-JANABI.

TABLE OF CONTENT

LIST OF TABLES

LIST OF FIGURES

LIST OF SYMBOLS

Δp	Pressure variance between chimney base and ambient (Pa)
Δp_t	Pressure variance at turbine (Pa)
Δp_f	Friction loss in the chimney (pa)
Δp_{in}	Entrance loss (pa)
Δp_{out}	Exit kinetic energy loss (pa)
ΔT	The temperature variance (K)
A_{ch}	Cross-sectional area of chimney (m^2) coefficient ($w/m^2.k$)
A_{coll}	Collector surface area (m^2)
c_p	Specific heat capacity of air (kJ/kg. k)
D_{ch}	Chimney diameter (m)
D_c	Diameter of collector (m)
f	The wall friction factor
G	Solar radiation (W/m^2)
g	Gravitational acceleration (m/s^2)
H_{ch}	Height of chimney (m)
H_c	Height of collector (m)
H_{Max}	Maximum chimney height (m)
H	Chimney height (m)
$\dot{m}$	Mass flow rate of air (kg/s)
P_i	Pressure inlet
P_o	Pressure outlet
P_{out}	Power generated by the turbine (W)
P_{Max}	Maximum power (W)
q	Heat transferred to air stream (W/m^2)
R_{coll}	Collector radius (m)
T_o	Ambient temperature (K)

U	Overall heat transfer
V	Velocity (m/s)
V_{ch}	velocity inner the chimney (m/s)
$V_{turb.i}$	velocity at turbine inlet (m/s)
$V_{ch,o}$	velocity at chimney exit (m/s)
v_{ch}	The air velocity at chimney inlet (m/s)
$V_{ch,max}$	The maximum velocity inside the chimney
$\dot{Q}$	Heat gain in the collector (W)
H_{ch}	Height of chimney
H_c	Height of collector
D_c	Diameter of collector
D_{ch}	Diameter of chimney
ET	Equation of time (min)
AST	Apparent Solar Time
L	Local latitude (^{o})
LL	Local longitude (^{o})
LST	Local standard time
DS	Daylight saving
pr	Prandtl number
SL	Standard longitude
T	Temperature (K)
N	Number of day
h	Number of minutes
Z	Solar azimuth angle (^{o})
H	Monthly average total radiation on the terrestrial horizontal surface (MJ/ m2).
Ho	Monthly average total radiation on the extraterrestrial horizontal surface (MJ/m2)
r_d	The ratio of hourly diffuse radiation to daily diffuse radiation.
h_{ss}	Sunset hour angle
r	The ratio of hourly total radiation to the daily total radiation

Greek Letters

β	Expansion rate
η	Efficiency
η_{tg}	Efficiency of turbine generator
η_{coll}	Solar collector efficiency
η_{Max}	Maximum efficiency
γ_{∞}	Lapse rate of temperature (K/m)
ε_{out}	Exit pressure loss coefficient
ε_{in}	Entrance pressure loss coefficient
ρ	Density (kg/m^3)
ρ_o	Ambient density (kg/m^3)
ρ_{ch}	The density of air at chimney inlet (kg/m^3)
ρ_{out}	Density of air at outlet of the chimney (kg/m^3)
δ	Solar Declination angle (^{o})

Subscripts

ch	chimney
c	collector
o	ambient
ch,o	outlet of the chimney
ch,i	inlet of the chimney
turb,i	turbine inlet

CHAPTER 1

LITERATURE REVIEW

1.1 Motivation and Aim of the Thesis Study

In recent years, the world's attention has been drawn to the danger of global warming, in part due to climate change in the form of floods and forest fires. These changes have led to economic problems such as oil and fossil fuel costs have risen. As a consequence, the demand has increased for clean energy developments such as solar energy. The solar energy is used in dwelling houses for heating the water and warming the house. Solar energy is able to produce electric current. Batteries store energy captured in daytime and supply power during the day. Solar energy is available everywhere without harmful emissions. Insight of the advantages of solar energy, in recent decades, new technology is developed upon the basic idea of the updraft solar heating known as Solar Chimney Power Plant (SCPP). It is a promising technology that is used to generate electricity from solar energy with high efficiency. The working principle of the solar chimney power plant is given in Figure 1.1.

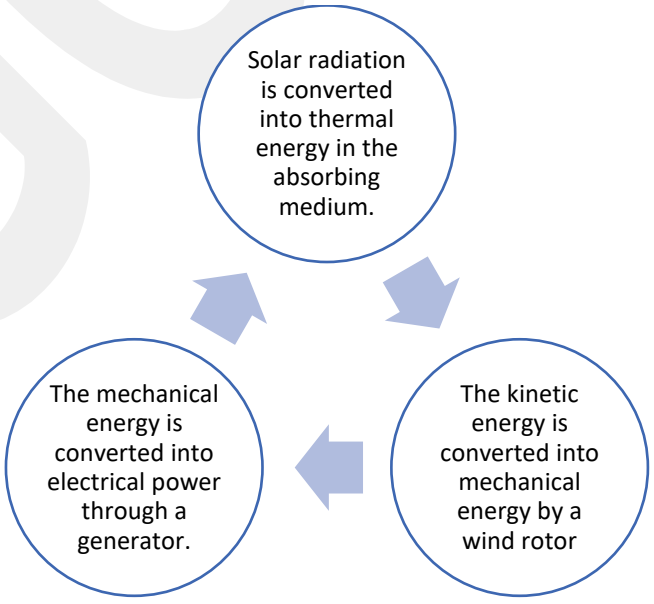

Figure 1.1. Working Principle of SCPP

In the first part of thesis, a parametric study is conducted to observe the effect of several parameters on SCPP performance. The parameters that are investigated are summarized below.

- Effect of chimney geometry on SCPP performance
- Chimney divergence angle effect on SCPP performance
- Effect of the ratio of chimney outlet diameter to chimney inlet diameter on SCPP performance.

In the second part of the thesis, the analysis and feasibility of implementing SCPP in Ankara, Turkey, is investigated under the climatic conditions in Ankara.

1.2 Introduction

1.2.1. Short History of the Energy

Energy, in whatever form it may take, is considered essential for our continued existence in the universe. Humans first began to utilize the thermal energy for warming and cooking. The heat energy created by a burning wood dissipates, and the dissipated heat warms the cold air around the fire. Wind and water drove the simple machines to ground the grain and pumping the water. In 10 AD. Hydropower was used by the Greeks to turn the water wheels. In 500AD. Windmills are developed in Persia for pumping the water. In the 17^{th} century, fireplaces were started to use in homes for warming and lighting. In the 1750s coal became the primary source of energy. In 1883, the first solar cell was developed by Charles Edgar Fritts. In 1949, King Hubbert claimed that fossil fuel would be evanished in one day and the human population should start to use other energy sources that are renewable. Insight of this, in 1958, the first full-scale nuclear power plant and 1978, the first multi-megawatt wind tunnel is constructed [1].

Newer forms of energy, such as natural gas and fossil fuels, as well as different techniques of harnessing it such as dams, nuclear power plants, and electrical power plants, have been constructed and continuing to settling for decades. While the benefits of harnessing such energy are many, there are also harmful results such as environmental pollution and global warming. Carbon dioxide emissions have negatively affected the ozone layer of the atmosphere, resulting in temperature changes. The gradual melting of the snow and ice in the northern parts of the globe

and the eruption of forest fires have been attributed to these atmospheric changes. It has become essential to reduce harmful emissions and to make investments and research and development studies in clean and renewable energy sources in order to preserve the environment. In recent years, the utilization rate of renewable energy has increased due to the increasing cost of oil and natural gas.

Wind and Solar energy play an important role in the decarbonization of electricity generation. Also, solar energy has great usage potential worldwide. Especially in the 20th century, solar energy became increasingly attractive because of its sustainability and its harmless meanwhile environmentally friendly. The capacity of solar energy is 200.000 times larger than the world's daily energy needs; therefore, solar energy has an enormous potential [2]. In the 1970s, China started to use solar energy in the beacon lights. In the 1990s, solar photovoltaic technology began to use. Nowadays, solar technology is used in our daily lives like solar traffic lights, solar street lamps, solar orientation lights and so forth. Solar energy is also used for public transportation such as trolleys, buses and light-rails [3]. According to the International Energy Outlook of 2010 [4], electricity generation will increase by 87% from 18.8 trillion kilowatt-hours in 2007 to 25.0 trillion kilowatt-hours in 2020 to 35.2 trillion kilowatt-hours in 2035. The proportion of electricity generation using renewable energy will increase from 18% in 2007 to 23% in 2035, as shown in Figure 1.2.

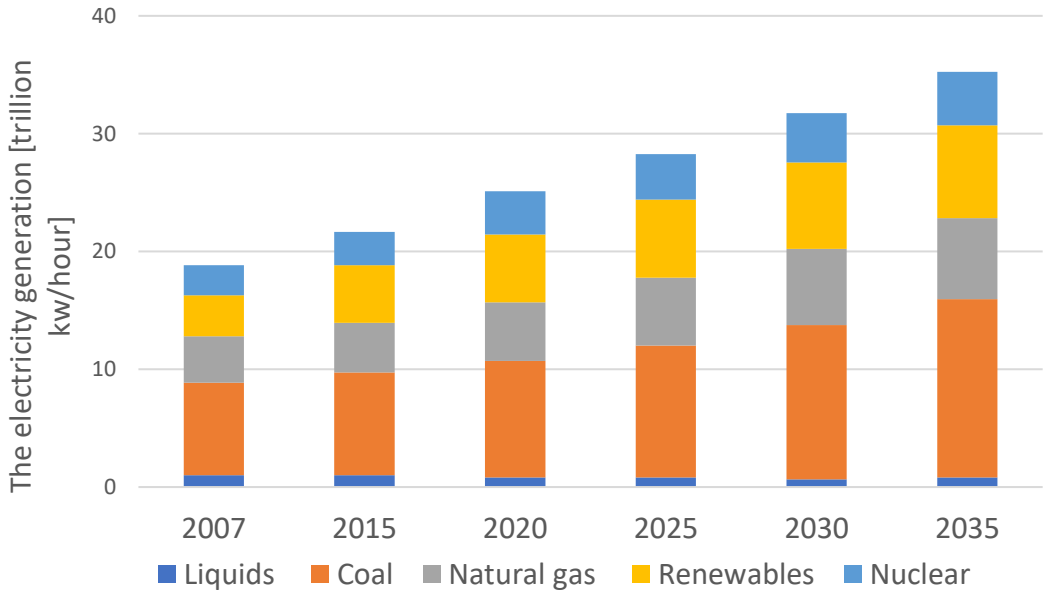

Figure 1.2: The electricity generation by energy source, 2007-2035 (trillion kilowatt-hours [adapted from 4]).

1.2.2. Renewable Energy

After the industrial revolution, there was an increase in energy demand. Power plants, as well as nuclear power stations, fossil fuels, and natural gas stations were built to meet this increased demand. Oil and coal were used which results in harmful emissions. These industrial and chemical stations which led to the generation of greenhouse gases like Methane CH_4, Carbon dioxide CO_2 and Nitrous oxide N_2O in addition to fluorinated gases caused damage to the ozone layer and consequentially causes global warming. Larger countries started to search for clean energy sources also known as sources of renewable energy in order to preserve the environment for posterity and to solve the issue of limited fuel sources which will eventually run out. Several conferences have been held to discuss how to reduce harmful emissions and how to develop further environmental protection [5]. Industrialized nations agreed on the Kyoto Protocol [6], which provides for the reduction of emissions in the coming years and the dependence on clean energy production.

Renewable energy is energy, which is collected from a natural source that does not never end and can be renewable within a human's lifetime. The most common clean energy examples are wind, solar, hydropower geothermal energy [7]. In the wind energy, with using the speed of the wind, wind turbines rotate and in this way, electricity is generated [8]. In the hydropower energy with using the head of the water, water turbines rotate according to the pressure difference. By using the hydraulic energy of the flowing water mechanical energy is generated. The mechanical energy is converted to the electricity [9].

Geothermal energy uses steam of water to produce energy with the injection of water into the ground; water is mutated to vapor, and the vapor pressure is used to rotate the turbines, tidal energy [10]. Solar energy is a bright light that comes from the sun. Several major applications of solar energy are solar water warming, solar heating of buildings, solar pumping, solar distillation, solar cooking, solar greenhouses [11]. Clean energy features no harmful emissions and offers environmental protection as well as the sustainability of human, plant, and animal wellbeing. It is never-ending and sustainable. In addition it is stable, safe, abundant and clean to use. In Figure 1.3, for 2018, total world energy consumption by the source is given [12]. The primary energy

sources in worldwide are coal and oil. According to the BP Statistical Review of World Energy [13], coal dropped from about 29% of the global total primary energy consumption in 2015 to 27% in 2017, and non-hydro renewables were up to about 4% from 2%. In Figure 1.4, contribution to primary energy growth for countries is shown. When it is compared with the last 5 years, growth in energy demand was 1.5 points higher in 2018.

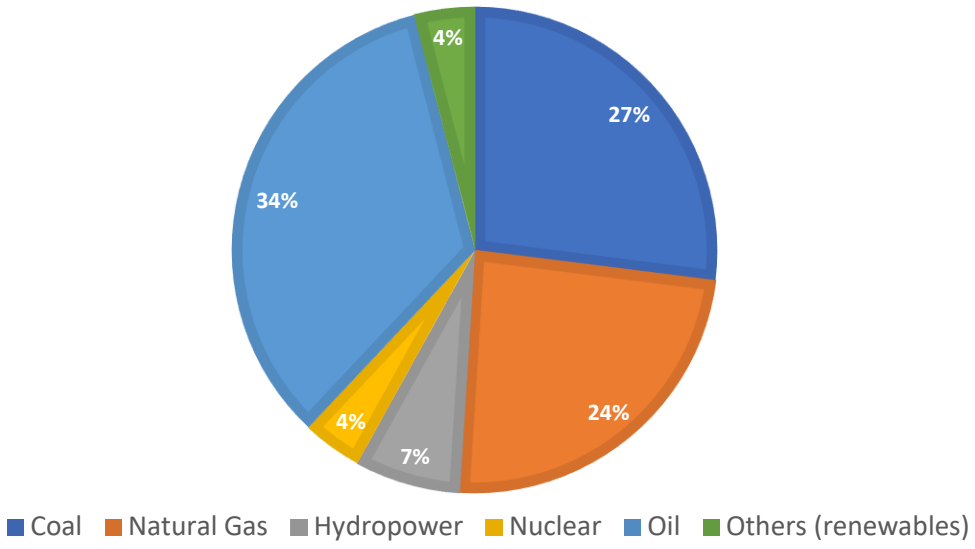

Figure 1.3: World total primary energy consumption by fuel in 2018 [adopted from 12]

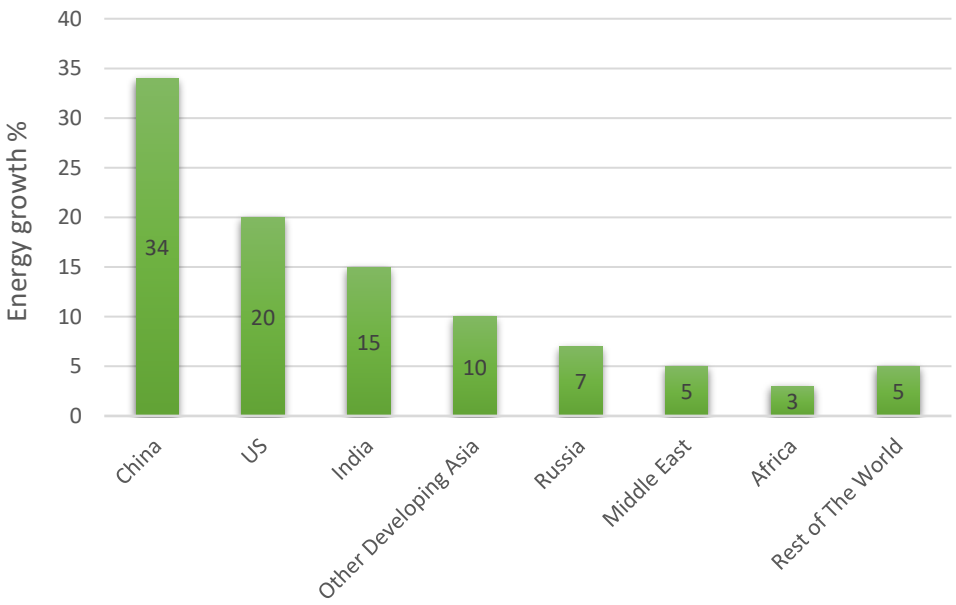

Figure 1.4: Contribution to primary energy growth in 2018 [adopted from 13]

1.2.3. Solar energy

In the worldwide, there is an increasing awareness that some realization of alternative energy sources can benefit the production of power and the solar energy is the most widespread among clean and renewable energy sources. There has been considerable interest shown by all the countries in solar energy, as it is the limitless, available, more easily harnessed, and totally non-polluting inexhaustible energy source that can be utilized economically to supply Man's energy needs for all time [14]. The sun is the main source of solar energy and its radiation can be exploited to generate heat and electricity. Solar energy is available in almost all countries because its technical requirements are minimal, and its maintenance costs are low. In addition, it is environmentally friendly and can be installed in big open spaces such as deserts. There are two applications, which are used to convert solar radiation to electricity. The first is an active solar technology with a pump and fan. This method can increase the efficiency of the system by helping to rotate the fluid within the system. The panel is made from semiconductor materials such as silicon. It is installed and follows the sun's movements in the sky, collecting the largest amount of radiation possible throughout the day.

The second technology is passive solar technology. Through the use of solar energy panels, which work to convert solar radiation to electric power without relying on external devices. The operating principle of passive solar panels is the transfer of heat from a warm face to a cooler face. The solar panel is put in windows, roofs, and walls and absorbs and stores solar energy. The main goal of this device is to get the maximum solar energy and use it to heat or cool the building, using the energy stored in the day which is converted at night into energy and light. There are many of these applications; one example is the solar power plant. In Figure 1.5, the schematic view of active and passive solar heating technologies is shown.

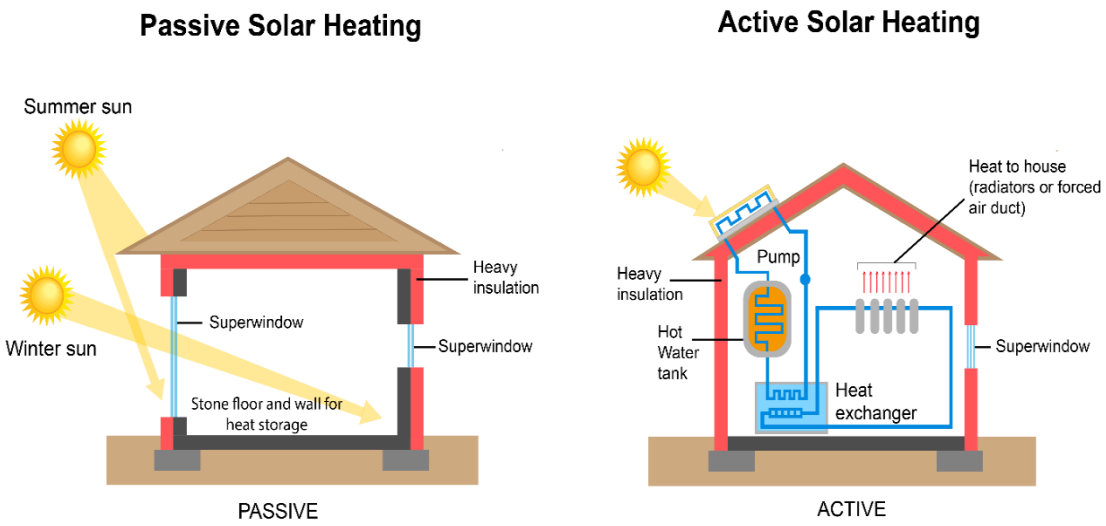

Figure 1.5: Active and Passive Solar Heating [15]

1.2.3.1. Solar Chimney Power Plants

Leonardo da Vinci sketched a smoke jack, which comprises four vanes. This machine uses the smoke or rarefied air, moving throughout the chimney and striking against the sails of the horizontal wheel. The effectiveness of this machine is a function of the chimney diameter and strength of the fire [16].

In 1903, The Spanish engineer Isidore Cabanyes [17,18], suggested a solar engine project to produce electricity. The device contents an air fireplace connected to a tower house and a wind fan that helped to rotate the propeller by the warm air. So, electricity is generated. In 1926, Dubois [19], suggested building a solar chimney power plant in North Africa. His main principle is using the solar chimney on the slope of the high mountain as shown in Figure 1.6. In 1931, Günther [20] analyzed the Dubos [19] suggestion about the possibility to reach air velocity 50 m/s in a chimney whose energy can be obtained from the wind turbines.

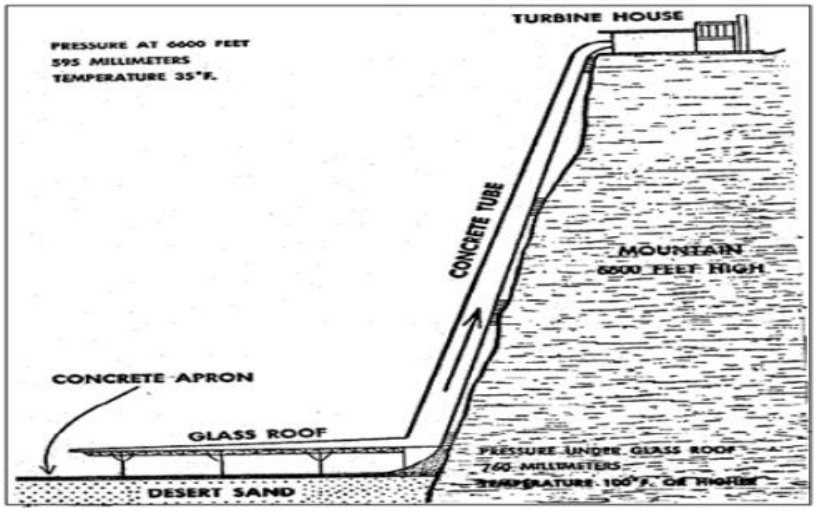

Figure 1.6: Principle of the Dubos's power plant [19]

In 1964, Nazare [21] proposed for the chimney of 100-300m rise with its geometry, such as a diffuser chimney. In 1982, a German team took the initiative and constructed a prototype of SCPP in Manzanares, Spain [22] that has 200 m chimney high and 50 kW generated power. In 2002, this project is chosen as the better discovery and most important in the year by Time Magazine [23]. The operating principle of the solar chimney station depends on the density change between warm air and ambient air. The solar radiation crosses through the collector ceiling and absorbed by the absorption layer. The air between the collector roof and the absorber layer is heated. As the hot air is light, it will rise up and due to density change between the hot air and cold air, the pressure difference is created. That difference led to turbine blades to rotate between outlet collector and inlet chimney and power is generated in this way [24]. The geometry of chimney area, height, and the geometry of collector affect the performance of SCPP [25]. Also, the ambient conditions, such as the amount of solar radiation and the air temperature have effect on amount of electricity production variation between the months of the year and between the hours on the same day has a direct influence on SCPP performance. The working principle of the solar chimney is shown in Figure 1.7.

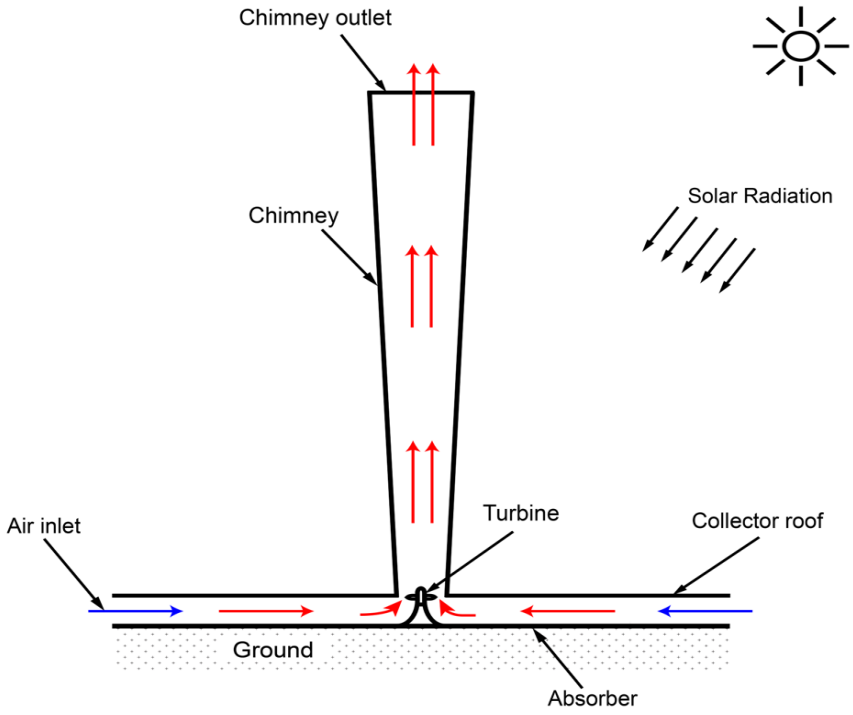

Figure 1.7: Schematic view of the working principle of the solar chimney

1.2.4. Components of Solar Chimney Power Plant

The chimney is the important part of a solar chimney power plant because the height, shape and diameter influence the performance of the system. Materials such as concrete and steel are used in the chimney. The chimney shape has a direct effect on the air velocity and amount of the air inside the system. According to the literature [26] and our previous studies the divergent chimney is the most efficient chimney configuration when it is compared with the standard, converging or converging-diverging chimney.

The main component in the SCPP is the solar collector, which is a special kind of heat exchange that produces hot air by the greenhouse effect. Collector height, collector diameter, and collector angle have impacts on the efficiency of the SCPP. It is diaphanous so it should be manufactured from glass or plastic which allowed to pass the largest amount of solar radiation. The material of the collector is chosen as a plastic layer or glass plastic layer. In Figure 1.8, the collector thermal balance scheme is shown. According to the figure, the ground under the roof heats up and transfuses the

heat to the flowing air. Natural convection, forced convection and solar radiation are takes place in the collector [23].

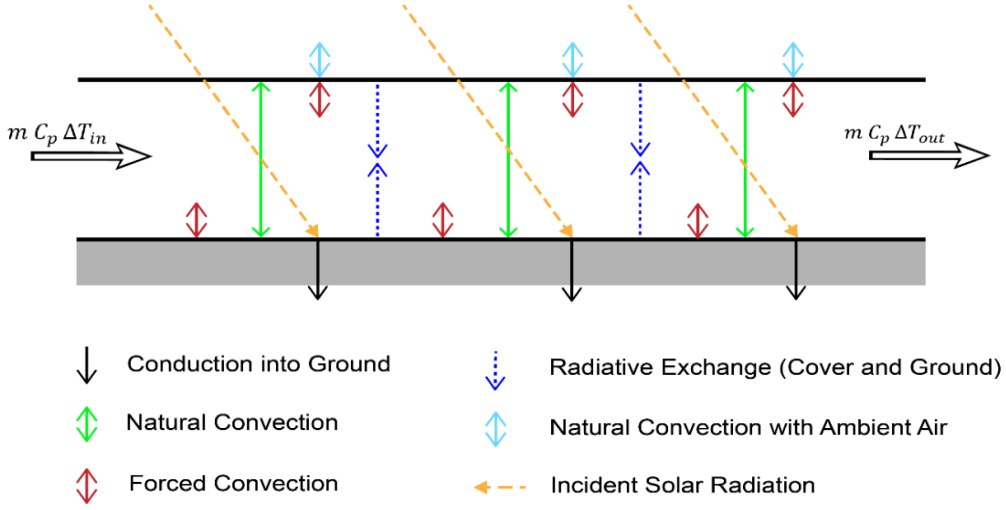

Figure 1.8: Thermal balance in solar chimney collector [23]

The turbine is one of the other major components of the solar chimney power plant as the turbine extracts the energy from the air and transfers it to the generator. The turbine is located at the base of the chimney, as at that point, velocity reaches its maximum value. Some system use one turbine while other system use multiple turbines depending on the chimney size. In Figure 1.9, the turbine location inside the chimney is shown.

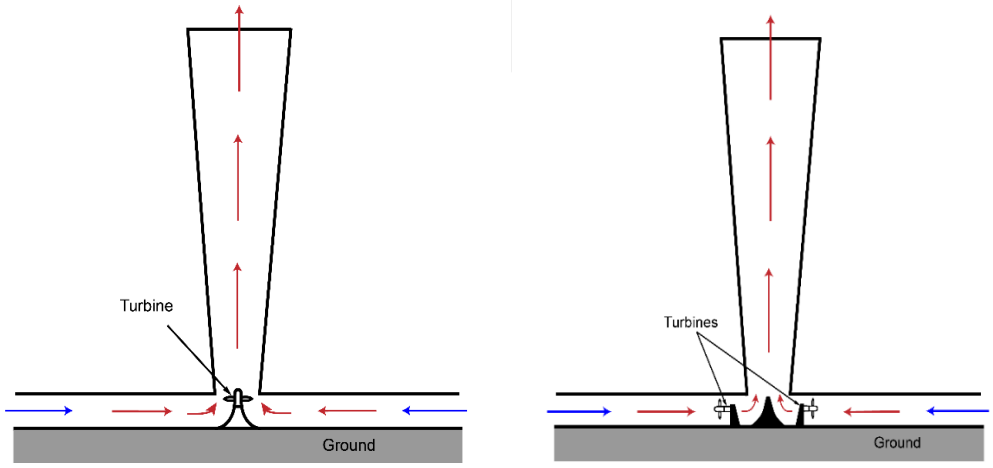

(a) (b)

Figure 1.9: (a) Single turbine inside the solar chimney. (b) Multiple turbines inside solar chimney.

1.3. Projects

In the recent years, great interest is developed for the solar chimney power plant because they are promising large-scale utilization of solar energy with an environmental-friendly approach, low maintenance and manufacturing costs. Based on the geographic and atmospheric conditions the feasibility of construction of SCPP is investigated. According to the feasibility studies, many countries, constructing SCPPs.

A solar chimney power plant was built in Manzanares city about Madrid in 1981-1982 by a German Company [27]. The solar chimney station has a 194.6 m height chimney with a diameter of 5.08. The collector radius is 122 m. The chimney supported by the wires because of the height. The turbine consists of four blades. The power production was 50 KW. The station worked 3197 hours in 1987. The purpose of the prototype was the investigation from the solve of the theoretical and studied the influence the meteorological conditions on the efficiency of the station. The Manzanares station has a capacity factor arrive in 10% but the researchers believe that would increase to 29% in a 200 MW unit. They used the plastic sheet glazing at the station but that be face with structural instability near the chimney because of the induced vortices. After 8 years of working, the tower support wires have become rusted and the tower felled because of the wind.

Pasumarthi and Sheriff [28,29], established a solar chimney experiment in 1997. The purpose of the project is to investigate the effectiveness of the chimney. The chimney height was about 7.92 m and the diameter gradually decreases from base 2.44 m and reach to the 0.61 m. The collector diameter 9.15m and the absorber layer is from the aluminum plate material. In Figure 1.10, the experimental set-up is shown. They found the collector area increase can improve efficiency and the temperature increase. Also they found the chimney height can affect the mass flow rate therefore efficiency increases.

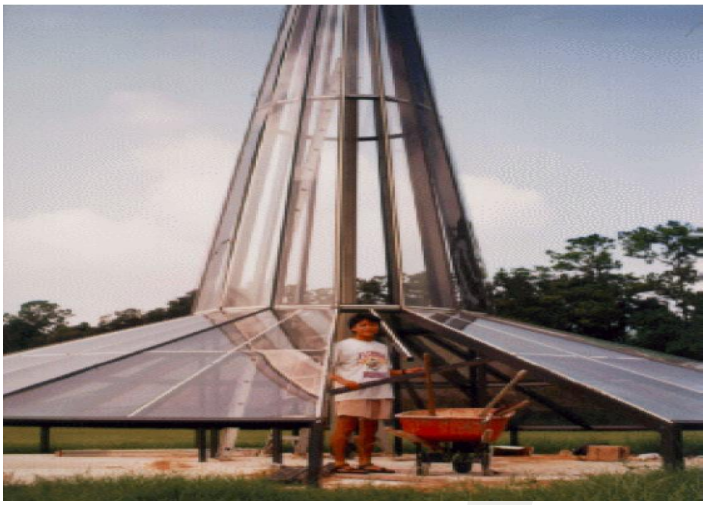

Figure 1.10: Pasumarthi Sheriff and Florida experiment [28,29].

In the HUST, China built an experimental solar chimney. The collector is a 5 m radius, a height of 0.05 m and the inclination angle for the collector is 8° [30]. They found that the solar radiation rises after sunrise, it is led to the air flow increase so power generation increases.

Koonsrisuk and Chinsomboon [31,32], built four small experimental models at the Suranaree University of Technology in Thailand. They established a numerical model and compare the results with experimental studies. In the first case, the fixed diameter chimney, with a height of 8 m, in the second case the divergent peak chimney, in the third case the fixed diameter chimney, and in the fourth case the half-size model of the first case is designed (Figure 1.11).

Case 1 Case 2

Case 3 Case 4

Figure 1.11: The experimental chimney configurations by Koonsrisuk and Chinsomboon [31,32].

In Tunisia in 2009 Higher Institute of Science and Energy Technology of Gafsa [33,34] built the first experimental solar chimney. The height of the chimney for each of them is 1.6 m and the diameter is 0.2 m that supported by steel wires. The roof collector is manufactured from Plexiglas and the inner cover is manufactured from the glass. Space between covers is 2.5 cm. They put 8 plates in the collector diametrically apart from 5.9 m each other. The collector has consisted of three circular rings. The angled slope for the collector is able to absorb a significant amount of solar radiation through the day [23].

Najmi et al. [35], built a small solar chimney to produce electrical power. The chimney height is 60 m and the diameter is 3 m. The collector is 40 m × 40 m with a square cross-section. The purpose of the study is to obtain maximum power with minimum costs. The results showed that using asphalt or rubber in the absorber layer, putting conic in the inlet of a chimney increases the generated power. Scientists and engineers have made several numerical studies and experimental work for SCPP in the world. They studied the effect of the geometry on the performance and compare the results with the Manzanares prototype. Some of the models SCPP show locations, dimensions, and the value of the results are presented in Table 1.1.

In 2009, the researchers [36] established a solar chimney model. The aim of the experiment is to measure the air temperature variation between the entrance and exit of the tower and improve the performance. The tower height is 4 m and the solar collector has 3 m radius. The result shows that the maximum air temperature difference is 22°C in the mid-day and the maximum velocity reaches to 2.309 m/s.

The Company Enviromission [37], build a solar chimney station in southwest Australia in 2001. The plant able to produce 4000 times more power than Manzanares station [23] with 200MW power generation. To reach such a power value, tower height is 1000m with a diameter of 130 m. The solar collector is 35 square kilometers to increase the warm air absorption that is required to operate the tower. The air velocity inside the collector is around 32 km/h and the air temperature is 30°C. The energy is obtained by using 32 turbines which has ten blades. The air temperature reaches around 60°C to 70°C before attacking to the turbines.

The solar chimney was built in the zone of Jinsha Bay Wuhai in inside Mongolia, China [38]. The project was an experimental prototype station with a 200 kW generated power. The first stage of the experimental prototype finished between May 2009 and December 2010. The project was covering an area of 40,000 m^2 of the wilderness. The tower has 53 m high and 18 m in diameter. The second stage started in February 2011 and finished in December 2011. The SCPP has 2.2 MW generated power that covers the area of 220,000 m^2 of the desert. The third stage of the project completed in December 2013 and the power capacity is 25.1 MW.

Bouabidi et al. [39], studied the impact of the chimney configuration on the performance of the solar chimney power plant (SCPP). The types of chimney geometry are changed numerically. The simulation included the four types of chimney configurations as standard, divergent, opposing, and convergent. According to the results, the chimney shape influences the efficiency of the SCPP. The maximum velocity is obtained at the center of the tower, gradually reduces along with the chimney in the standard chimney. The location of the maximum velocity was at the top of the chimney in the convergent chimney. With the opposing chimney, the maximum velocity appeared at the middle of the chimney due to the decrease of the diameter and consequent decrease in velocity. In the divergent chimney, the maximum

velocity occurred at the inlet of the chimney and exceeded that of the standard chimney.

Hu et al. [40], proved that the solar chimney station was directly affected by the change in the chimney shape from a cylinder chimney to a divergent chimney. The effect of the ratio of the area of the chimney outlet to the area of chimney inlet is investigated. Also, the effect of changing the divergent inclination angle of the chimney wall is studied numerically. A verification study is performed using the Manzanares pilot plant [34]. According to the results, system performance increases with the divergent chimney that has a more mass flow rate than the cylinder chimney.

Larbi et al. [41] studied the impact of solar radiation, change of the tower rise, and roof of the collector on electricity production especially in remote areas. The results showed that the power generation relies on chimney height, amount of irradiance, collector area, and ambient temperature. The solar radiation amount has a greater effect on the system than the effect of ambient temperature. The turbine and collector have an effect on the enhancement of efficiency and enhancement of the system performances. The solar heat collector can be benefited as a greenhouse for agricultural purposes.

Sangi [42], established a mathematical model and estimate the efficiency of the solar chimney power plants in several cities in Iran theoretically and measured the generated electricity from the system, studying the influence of change in the parameters and several ambient conditions. The result showed that a solar chimney power plant with 1000 m diameter for the collector and a 350 m chimney rise able to power generation a monthly average of 1-2 MW over a year. Through this study, power generation was studied in five locations in Iran, namely, Abadan, Arak, Tehran, Yazd, and Zanjan. The results showed that the amount of power generated depends on ambient temperature, chimney rise, collector radius, and solar radiation. When the tower height is increased, the collector size, the amount of solar radiation, and the power generation capacity will also increase.

Bernardes et al. [43] studied the impact of structural dimensions and the different surrounding conditions on the power output with establishing a mathematical model to analyze the influence on the performance of solar chimney stations. They compare their results with experimental data from a prototype in Manzanares. The results

showed that the rise of the chimney, the collector diameter, the transmittance of the collector and directly affects the power output.

Çağlar et al. [44], studied the quantity of global radiation and beamed radiation from May 2008 to May 2009 in Ankara city. They also analyzed and recorded the amount of radiation it used hourly, daily, and monthly in Ankara, comparing the observed amounts with the results of various other cities in Turkey. The results showed that in May, the global radiation was 1056 W/$m^{2,}$ and beamed radiation in the same month was 1010 W/m^2. The recorded maximum daily and average global radiation is 383 W/m^2 for May and in July, the average was 348 W/m^2. The air temperature on July 23, 2008, was 36.6°C and the maximum daily average temperature on Jule 24 in 2008 was 28.9°C. The data were compared with the data of the State Meteorological Service in Ankara and it was observed that there is a need to improve the network map and to amend and correct the values of the solar potential of Ankara.

Ghonemy [45] established a mathematical model to calculate and analyze the parameters that have a direct impact on the solar chimney performance like pressure drop, optimum tower height, air velocity, and air temperature. The results showed that with rise of a tower of 200 m and a diameter of 10 m, the electric power would be 118-224 kW. This value is the monthly rate of power production in the year. It proved that the rise of the chimney and collector radius would increase the power capacity.

Ayadi et al. [46], studied the influence of the collector layer slope on the performance of the solar chimney. The results showed that the efficiency of the system will increase with the negative collector angle and increase in the velocity inside the solar station will increase the power output. Also, a satisfactory similarity was observed among the numerical results and experimental results.

Patel et al. [47], studied the effect of the geometries of the parts of the solar chimney station on performance by using the ANSYS-CFX software. They concluded that increasing the collector height increases the efficiency of the power plant.

Table 1.1 Some of experimental set up for SCPP in the world

N	LOCATION	Chimney Height (m)	Chimney Diameter (m)	Collector Diameter (m)	Collector material	V (m/s)	ΔT	Ref
1	Baghdad-Iraq	4	0.2	6	-	2.31	22	36
2	Zanjan Iran	12	0.25	10	Plastic	2.9	26	48
3	Karak Jordan	4	0.58	$36m^2$	Plastic	-	-	49
4	Florida USA	7.92	2.44-0.61	9.14	Plastic	3.1	28	28 29
5	Izmir Turkey	2	0.07	$9m^2$	-	-	-	50
6	Kerman Iran	60	3	$40*40m^2$	Glass	-	-	51
7	Wuhan China	15	1.2	10	Glass	2.8	24.1	52
8	Adiyaman, Turkey	17.15	0.8	27	Glass	5.5	26	53
9	Alain UAE	8.25	0.25	$10*10m^2$	Plastic	-	-	54
10	Damacus, Syria	9	0.31	12.5	Glass	2.9	19	55
11	Gafsa, Tunisia	16	0.4	15	Glass+ Plastic	-	-	56
12	Belo, Brazil	12.3	0.1	25	Plastic	2.9	27	57
13	Gaborone, Bostwana	22	2	$15*15$ m^2	Glass	22	6.8	58

CHAPTER 2

METHODOLOGY

2.1 Mathematical Modelling

The main objectives of this thesis are investigating the effect of the divergence angle on SCPP performance and optimizing the energy conversion within the solar chimney from power density. For this purpose, numerical studies are carried out. The two-dimensional, incompressible, steady state Navier-Stokes equations are solved with using ANSYS FLUENT software with using Reynolds-Averaged Navier-Stokes model. The continuity equation, and the energy equation with a second-order upwind discretization and a pressure-based coupled algorithm is utilized to the problem. The buoyancy effects are implemented using the Boussinesq model. The mathematical model of the plant is based on the following assumptions.

2.1.1 Assumption

- Steady-state operation
- Air is used as an ideal gas and there is no evaporation inside the tower.
- The Boussinesq approximation is used for modeling the buoyancy-driven flow.

2.1.2 Solar Chimney Performance Equations

The efficiency of the solar chimney power plant can be calculated by using the following equation [49],

$$\eta_{coll} = \frac{\dot{m}\, C\dot{p}\, \Delta T}{A_{coll}\, G} \quad (1)$$

Where $\dot{m}$ is the mass flow rate of the warm air inside the chimney, c_p is the specific heat capacity for the air, ΔT is the temperature difference between the warm air inside

the collector and ambient air, A_{coll} is the area of the collector and G is solar radiation on the collector.

$$\dot{m} = V_{ch}\, A_{ch}\, \rho_{ch} \tag{2}$$

ρ_{ch} indicates the density of air, V_{ch} is the air velocity in the chimney and A_{ch} is cross area of the chimney.

Substituting Equation (2) in Equation (1), we obtain

$$\eta coll = \frac{V_{ch}\, A_{ch}\, \rho_{ch}\ \dot{m}\, Cp\, \Delta T}{A_{coll}\, G} \tag{3}$$

On the other hand, to find the pressure difference between the chimney base and the ambient Equation (4) is used [59],

$$\Delta p = 0.00353\, g\, H \left(\frac{\pi\, G\, \eta_{coll}}{C_p\, \dot{m}}\ R_{coll}^2 - \frac{g}{2\, C_p} H + \frac{1}{2} \gamma\ H\right) \tag{4}$$

Where g is gravitational acceleration, H is the chimney height, R_{coll} indicates collector radius, γ is the lapse rate of air temperature.

The turbine pressure drop can be calculated as [60],

$$\Delta p_t = \Delta p - \Delta p_f - \Delta p_{in} - \Delta p_{out} \tag{5}$$

And the pressure loss of the chimney is obtained from the equation

$$\Delta p_f = f \frac{H}{D} \frac{1}{2} \rho\, V_{ch}^2 \tag{6}$$

where f is Fraction factor, D is chimney diameter, ρ is the air density and V_{ch} is the air velocity inlet the chimney .

V_{ch} is calculated from the below Equation;

$$V_{ch} = \sqrt{\frac{2g\, H\, \Delta T}{T_o}} \tag{7}$$

Where T_o is ambient temperate.

Entrance loss, Δp_{in} is obtained from the equation [60],

$$\Delta p_{in} = \varepsilon_{in}\ \frac{1}{2} \rho\, V_{turb,i}^2 \tag{8}$$

Where ε_{in} is pressure loss coefficient. Turbine velocity inlet $V_{turb,i}$ can be calculated from the equation;

$$V_{turb,i} = \sqrt{\frac{2\,g\,H\,\Delta T}{3\,T_o}} \tag{9}$$

Δp_{out} can be obtained from the equation [53],

$$\Delta p_{out} = \varepsilon_{out}\,\frac{1}{2}\,\rho out\,V_{ch,o}^2 \tag{10}$$

Where ρ_{out} is indicative of the density of air outside the chimney, ε_{out} is exit pressure loss coefficient and $V_{ch,o}$ is calculated by using the equation [60],

$$V_{ch,o} = V_{ch}\,(\frac{A_{ch}}{A_{ch,o}}) \tag{11}$$

The power output of the turbine (P_{out}) is calculated by the equation [60],

$$P_{out} = \eta_{tg}\,\Delta P_t\,V_{ch.max}\,A_{ch} \tag{12}$$

Where η_{tg} is the efficiency of turbine and $V_{ch.max}$ is maximum velocity inside the chimney. To obtain $V_{ch.max}$ the following equation can be used;

$$V_{ch.max} = \sqrt{\frac{2\,g\,H_{ch}\,\Delta T}{T_o}} \tag{13}$$

The total efficiency of solar chimney power plant is defined as [60],

$$\eta = \frac{P_{out}}{\pi\,R_{coll}^2\,G} \tag{14}$$

The maximum height of the chimney power plant can be calculated by the equation;

$$H_{Max} = \frac{c_p\,\dot{m}}{U\,\pi\,D}\,\ln\,(\frac{\pi^2\,U\,D\,\eta_{coll}\,R_{coll}^2}{c_p\,\dot{m}^2\,(g-\gamma_\infty\,c_p)}) \tag{15}$$

Where, η_{coll} is solar collector efficiency and U is overall heat loss coefficient.

2.2 Solar Energy Equations and Solar Angles

2.2.1 Equation of time (ET)

The earth is rotating around the sun in an elliptical orbit because of the difference orbital velocity during the year therefor AST difference a little from the mean time.

The variation is called the equation of time (ET). the earth is revolution around itself 24 hours but it is not uniform during the year because of the elasticity of the orbit [61].

$$ET = 9.87\sin(2B) - 7.53\cos(B) - 1.5\sin(B) \ \text{[min]} \quad (16)$$

$$B = (N - 81)\frac{360}{364} \quad (17)$$

Where N is the number of day of the year.

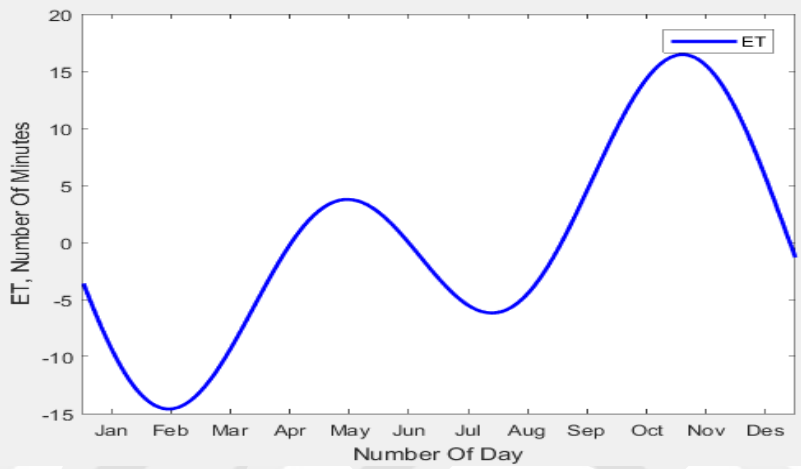

Figure 2.1: Monthly equation of time graphic [61].

2.2.2 Longitude Correction.

The sun requires 4 minutes to cross 1° of longitude, therefor the longitude correction is equal to 4*(standard longitude – local longitude).

2.2.3 Apparent Solar Time (AST).

The equation is used to calculate the apparent solar time

$$AST = LST + ET \mp 4(SL\text{-}LL) - DS \quad (18)$$

Where

LST, local standard time. ET, Equation of time. SL, Standard longitude (meridian, 30 for Turkey). LL, Local longitude (32.8^{o} east for Ankara). DS, Daylight saving.

2.4.4 Solar Angles

The earth is rotating around itself once through 24 hours and it's rotating around the sun during 365 days in an elliptical orbit, which let the four-season occur. The distance between the sun and the earth in the summer season is (152.1×10^6 Km) and in the winter season, the distance is (147.1×10^6 Km). The sun locations in the sky varies between the sunrise to sunset. The earth is rotation around itself is tilted at an angle (23. 45˚) [61]. As shown in Figure 2.2. and Figure 2.3.

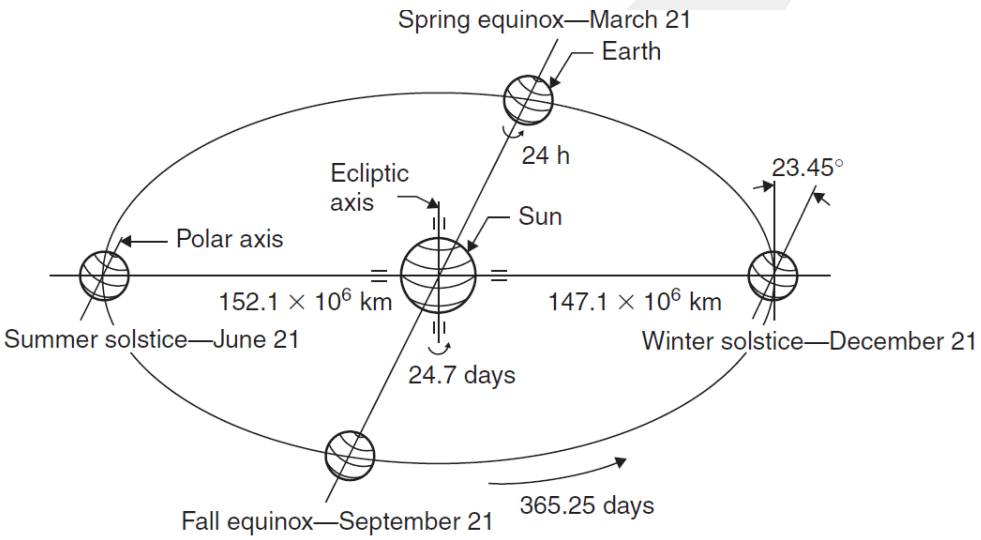

Figure 2.2: The annual movement of the earth around the sun [61].

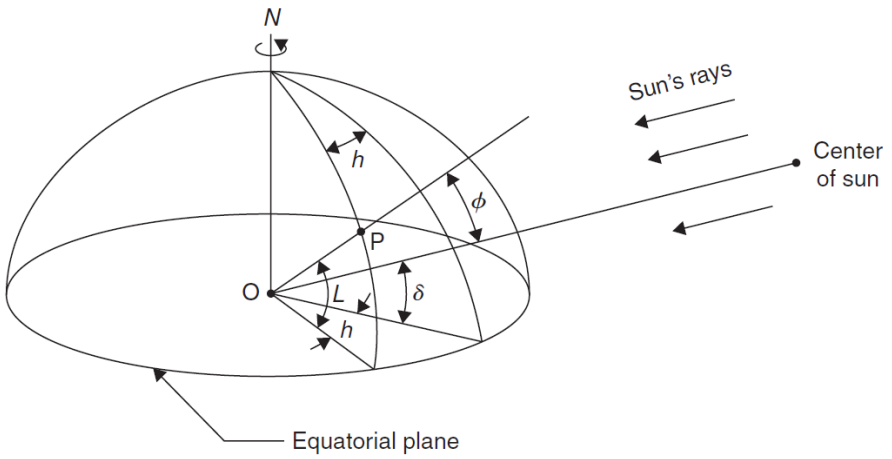

Figure 2.3: Latitude (L), hour angle (h), and solar declination angle [61].

2.2.4.1 Solar Declination

The solar declination is the angle between the line connecting the earth center and the sun and its projection on the equatorial plane. The declination is changing due to the

earth rotation around the axis which led to the angle ranges between 23.45 at the summer solstice and -23.45 at the winter solstice**.** The Solar declination can be obtained by [ASHRAE, 2007] equation [61]. As shown in Figure 2.4.

$$\delta = 23.45\, sin\frac{360}{365}\,(284 + N) \tag{19}$$

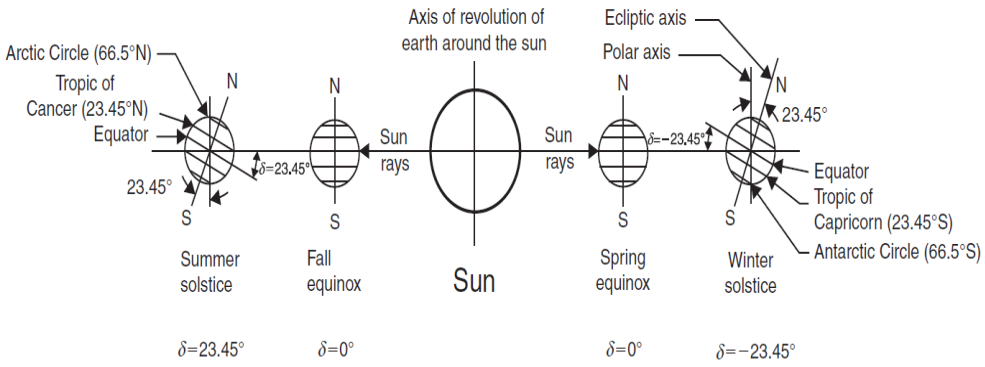

Figure 2.4: Annual variation of the solar declination angle [61].

2.2.4.2. Hour Angle (h)

Hour angle is the angle which is necessary to turn any position of the earth to the meridian. The result of the earth rotation around its axis by 15 degrees corresponds to one hour which the afternoon being positive morning being negative and in the noon is equal zero. The Figure 2.3 shows the hour angle which can obtain by using the equation [61].

$$\text{h} = \mp 25\ (\text{Number of minutes}) \tag{20}$$

Or can be calculated from AST,

$$\text{h} = (\text{AST-12})\ 15 \tag{21}$$

2.2.4.3 Solar Altitude and Solar Zenith Angle (α & ϕ)

The solar altitude angle is the angle between the sun's radiation and horizontal plane. The angle is zero at sunrise and gradually increase until reaching a maximum at the

noon after that reduce to zero at sunset. Zenith angle is the angle between the sun's rays and the vertical as shown in Figure 2.5.

$$\sin(\alpha) = \cos(\phi) = \sin(L)\sin(\delta) + \cos(L)\cos(\delta)\cos(h) \quad (22)$$

And

$$\phi + \alpha = 90 \quad (23)$$

Where, L is Local latitude

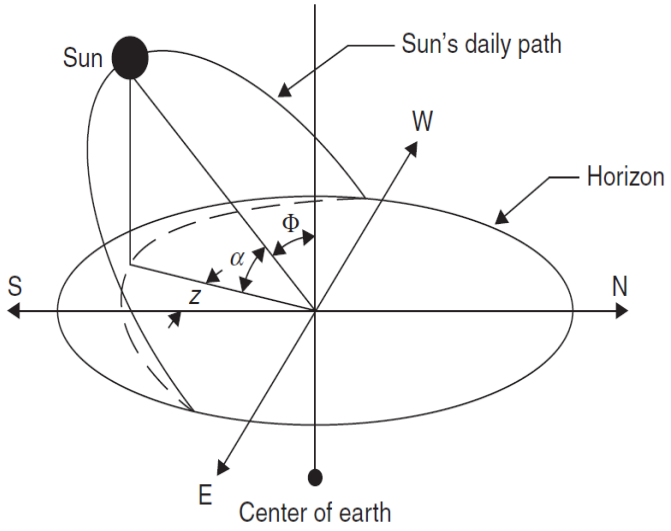

Figure 2.5 The movement of the sun across the sky during the day [61].

2.2.4.4 Solar Azimuth Angle (z)

The solar azimuth angle is the angle between the solar projection line on the horizontal plane and the line corresponding to the south direction. The angle is negative in the morning while being positive in the afternoon and equal zero at noon [61].

$$\sin(z) = \frac{\cos(\delta)\sin(h)}{\cos(\alpha)} \quad (24)$$

2.2.4.5 Sunrise and Sunset

At the sun rise and sun set, the altitude angle is equal zero so the equation will be as follows:

$$\sin(\alpha) = \sin(0) = 0 = \sin(L)\sin(\delta) + \cos(L)\cos(\delta)\cos(h_{ss}) \quad (25)$$

$$\cos(h_{ss}) = \frac{-\sin(L)\sin(\delta)}{\cos(L)\cos(\delta)} = -\tan(L)\tan(\delta) \quad (26)$$

Where

h_{ss} is positive at sunset. H_{ss} and H_{sr} are the sun-set and sun rise from local solar noon (hour).

$$H_{ss} = -H_{sr} = \frac{1}{15}\cos^{-1}[\tan(L)\ \tan(\delta)] \quad (27)$$

$$\text{Day length} = \frac{2}{15}\cos^{-1}[\tan(L)\tan(\delta)] \quad (28)$$

2.3 Solar Radiation

The global solar radiation quantity is important to operate the solar chimney power plant. In fact, the Meteorological station is measuring the solar radiation by using the pyranometer as shown in Figure 2.6 [61]. The device used to measure the beam and diffuse solar radiation within the hemispherical domain of view. The total solar radiation is the sum of beam radiation (direct solar radiation), diffuse radiation (solar radiation coming to the earth after scattering by the atmosphere) and reflected solar radiation. In the summer season it has the highest daily maximum global radiation (solar rays reflected from the surrounding) while the winter season has a lower amount due to climate fluctuations and clouds that effect on the beam radiation and diffuse radiation. Table 2.1 shows the amount of average global radiation in some cities in Turkey [44].

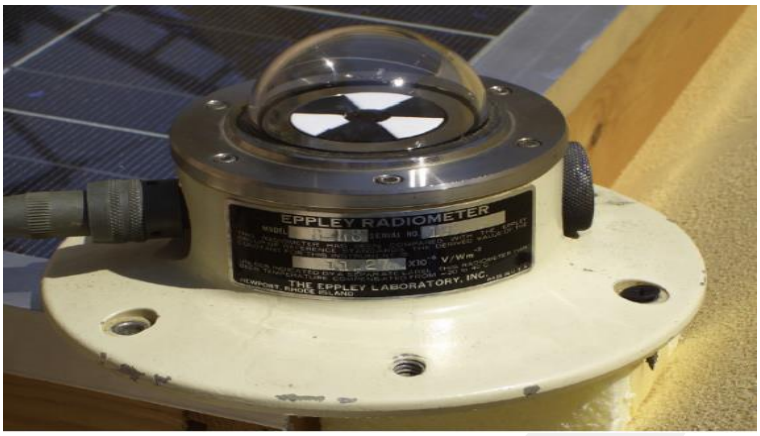

Figure 2.6: The pyranometer device [61].

Table 2.1: Monthly and yearly average daily total solar radiation for Ankara and some cities in Turkey [44].

Stations	May	Jun	Jul	Aug	Sep	Oct	Nov	Dec	Jan	Feb	Mar	Apr	Annual
Monthly and annual average global radiation in MJ/m²/day													
Ankara, METU May 08-Apr. 09	24,13	29,05	30,11	26,65	18,33	13,64	9,01	6,61	7,01	8,23	12,46	19,25	17,04
Ankara, SMS May 08-Feb. 09	22,41	26,88	27,92	24,72	16,78	12,53	7,99	5,63	6,12	7,42	11,35	17,73	15.62
Ankara 14-year average	21,86	24,25	24,91	21,92	17,62	12,13	7,64	5,45	6,28	9,61	13,57	17,30	15,26
Antalya 14-year average	22,65	24,95	24,47	22,00	18,97	13,86	9,38	6,99	8,13	11,29	15,66	18,93	16,44
İstanbul 14-year average	21,38	23,60	23,36	19,69	15,64	10,14	6,24	4,34	5,13	7,99	11,85	16,17	13,79
İzmir 12-year average	23,92	26,72	26,24	23,54	19,23	14,03	9,31	6,61	7,88	10,87	15,34	18,94	16,88
Trabzon 14-year average	17,22	18,67	17,22	14,43	12,53	8,76	6,47	4,90	5,61	8,09	10,73	13,62	11,49
Van 13-year average	25,42	29,06	27,79	25,25	21,48	15,14	11,04	8,83	10,29	14,05	17,96	20,68	18,86

2.3.1 Hourly Solar Radiation Calculation

Since the data we have is average daily solar radiation, hourly radiation values should be calculated using following formula. Firstly, monthly average index clearance is calculated as:

$$K_T = \frac{H}{H_O} \tag{29}$$

Where, H; Monthly average total radiation on the terrestrial horizontal surface, H_0; Monthly average daily total radiation on the extraterrestrial horizontal surface.

Secondly, ratio of diffuse radiation to total radiation is calculated as:

$$\frac{H_D}{H} = 1.39 - 4.027\ \overline{K}_T + 5.531\overline{K}^2_T - 3.108\ \overline{K}^3_T \tag{30}$$

By using Liu and Jordan relation [61];

$$r_d = \frac{\text{average hourly diffuse radiation}}{H_D} = \left(\frac{\pi}{24}\right)\frac{\cos(h) - \cos(h_{ss})}{\sin(h_{ss}) - \left(\frac{2\pi h_{ss}}{360}\right)\cos(h_{ss})} \quad (31)$$

Where;

r_d= The ratio of hourly diffuse radiation to daily diffuse radiation.

h_{ss}= sunset hour angle.

h = Hour angle in degrees at the midpoint of each hour.

And according to the Collares-Pereira and Rabl [61] relation.

$$r = \frac{\text{average hourly total radiation}}{H} = \left(\frac{\pi}{24}\right)[\alpha+\beta\cos(h_{ss})]\left(\frac{\cos(h)-\cos(h_{ss})}{\sin(h_{ss})-\left(\frac{2\pi h_{ss}}{360}\right)\cos(h_{ss})}\right) \quad (32)$$

r = the ratio of hourly total radiation to the daily total radiation.

$$\alpha = 0.409+0.5016\sin(h_{ss}-60) \quad (33)$$

$$\beta = 0.6609-0.4767\sin(h_{ss}-60) \quad (34)$$

2.4. Numerical Solution

2.4.1 Navier -Stokes Equations

The Navier-Stokes equations are the equations rule the motion of fluids and can be considered as Newton's second law of motion for the fluids. The Navier-Stokes equations represent the conservation of momentum, while the continuity equation represents the conservation of mass.

The continuity equation for 2-D and steady-state flow field can we written as

$$\frac{\partial(\rho u)}{\partial x} + \frac{1}{r}\frac{\partial(r\rho v)}{\partial r} = 0 \quad (35)$$

Where ρ is density of the air, u is velocity in x-direction and v is velocity in radial direction.

The momentum equations for steady state and 2D flow in cylindrical coordinates can be written as:

$$\frac{\partial(\rho uu)}{\partial x}+\frac{1}{r}\frac{\partial(r\rho uv)}{\partial r}=\frac{\partial p}{\partial x}+(\rho-\rho_o)g+\frac{\partial}{\partial x}\left[(\mu+\mu_t)\frac{\partial u}{\partial x}\right]+\frac{1}{r}\frac{\partial}{\partial r}\left[(\mu+\mu_t)r\left(\frac{\partial u}{\partial x}+\frac{\partial v}{\partial r}\right)\right] \quad (36)$$

$$\frac{\partial(\rho uv)}{\partial x}+\frac{1}{r}\frac{\partial(r\rho vv)}{\partial r}=-\frac{\partial p}{\partial r}+\frac{\partial}{\partial x}\left[(\mu+\mu_t)\left(\frac{\partial v}{\partial x}+\frac{\partial u}{\partial r}\right)\right]+2\frac{1}{r}\frac{\partial}{\partial r}\left[(\mu+\mu_t)r\frac{\partial v}{\partial r}\right]-\frac{2(\mu+\mu_t)}{r^2} \quad (37)$$

Where P is pressure, μ is kinematic viscosity, g is gravitational acceleration and μ_t is defined as chimney top's kinematic viscosity coefficient.

The energy equation can be written as follows;

$$\frac{\partial uT}{\partial x}+\frac{1}{r}\frac{\partial(rvT)}{\partial r}=-\frac{1}{\rho}+\frac{\partial}{\partial x}\left[\left(\frac{\mu}{p_r}+\frac{\mu_t}{\sigma_t}\right)\frac{\partial T}{\partial x}\right]+\frac{1}{\rho r}\frac{\partial}{\partial r}\left[\left(\frac{\mu}{p_r}+\frac{\mu_t}{\sigma_t}\right)r\frac{\partial T}{\partial x}\right] \quad (38)$$

Where, σ_t is an indicative of turbulent Prandtl Number.

The buoyancy force for the solar chimney is modeled based on Boussinesq Approximation which can be found below:

$$(\rho-\rho_o)\,g=\rho_o\,\beta(T-T_o)g \quad (39)$$

Where β is the thermal expansion rate.

2.4.2 Turbulence Model

The Rayleigh Number is product of Prandtl Number which shows the connection between momentum diffusivity and thermal diffusivity, and Grashof number which shows the connection between buoyancy and viscosity in a fluid. The Rayleigh number can be obtained from the Eq.

$$Ra = Gr.\,Pr \quad (40)$$

Rayleigh number is related with buoyancy force also called natural convection. The Rayleigh number value describes the type of flow inside the channel. If the flow Rayleigh number is 10^6 and less of that, flow is said to be laminar, if Rayleigh number is between 10^6 and 10^7, it is transition and if Rayleigh number is greater than 10^7, flow is said to be turbulence flow [62] as shown in Figure 2.7.

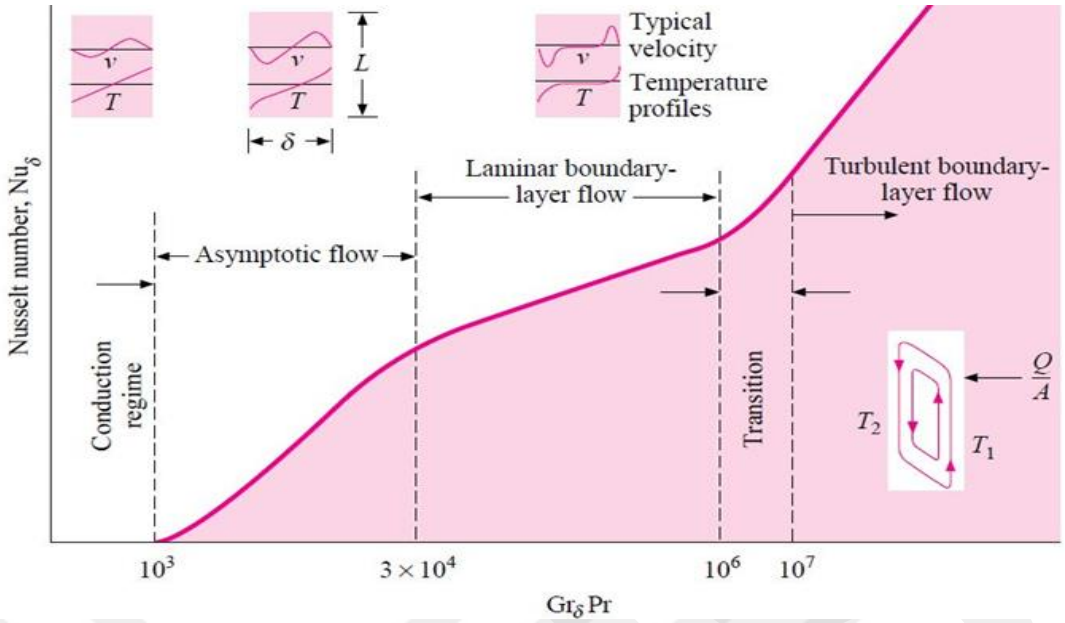

Figure 2.7: Show schematic diagram for flow types [63].

Ra can be written as below:

$$Ra = \frac{g\,\beta\,\Delta T}{v^2}\, L^3.\, Pr \tag{41}$$

Where g is acceleration due to gravity, β is Thermal expansion coefficient, ΔT is temperature difference between inlet and outlet for the air an v and L are kinematic viscosity of the fluid and characteristic length respectively. In fact, the flow inside solar chimney is turbulent flow since $Ra=8x10^8$.

2.4.3 Standard K-ε Turbulence Model

K - ε is one of the most commonly used turbulence model in Computational Fluid Dynamics and focuses on the Kinetic energy. Where, the K is turbulent kinetic energy and ε is turbulence kinetic energy dissipation [64].

$$K = \frac{1}{2}(U^2 + V^2 + W^2) \tag{42}$$

$$K = \frac{1}{2}(\acute{u}^2 + \acute{v}^2 + \acute{w}^2) \tag{43}$$

$$k(t) = K + k \tag{44}$$

$$\nu_t \propto \vartheta \ell \propto k^{1/2} \frac{k^{3/2}}{\varepsilon} = \frac{k^2}{\varepsilon} \quad (45)$$

Where; ε is the dissipation rate of k, ν_t is kinematic turbulent viscosity, ϑ is indicative of velocity scale and ℓ is the length scale.

The k- ε can be obtained from the equations,

$$\frac{\partial(uk)}{\partial x} + \frac{1}{r}\frac{\partial(rvk)}{\partial r} = \frac{1}{\rho}\frac{\partial}{\partial x}\left[\left(\mu + \frac{\mu_t}{\sigma_k}\right)\frac{\partial k}{\partial x}\right] + \frac{1}{\rho r}\frac{\partial}{\partial r}\left[\left(\mu + \frac{\mu_t}{\sigma_k}\, r\, \frac{\partial_k}{\partial_r}\right)\right] + G_k - \varepsilon \quad (46)$$

$$\frac{\partial(u\varepsilon)}{\partial x} + \frac{1}{r}\frac{\partial(rv\varepsilon)}{\partial r} = \frac{1}{\rho}\frac{\partial}{\partial x}\left[\left(\mu + \frac{ut}{\sigma\varepsilon}\right)\frac{\partial \varepsilon}{\partial x}\right] + \frac{1}{\rho r}\frac{\partial}{\partial r}\left[\left(\mu + \frac{\mu_t}{\sigma_\varepsilon}\right)\right] + \frac{\varepsilon}{k}\left(C_1 G_K - C_2 \varepsilon\right) \quad (47)$$

Where,

The Constant, $C_1 = 1.44$, $C_2 = 1.92$, $\sigma_\varepsilon = 1.3$, $C_\mu = 0.09$ and $\mu_t = \frac{c_\mu \rho k^2}{\varepsilon}$

G_k is the generation of turbulence kinetic energy and we can calculate

$$G_k = -\mu_t\left(2\left(\left(\frac{\partial u}{\partial x}\right)^2 + \left(\frac{\partial v}{\partial r}\right)^2 + \left(\frac{v}{r}\right)^2\right) + \left(\frac{\partial u}{\partial r} + \frac{\partial v}{\partial x}\right)^2\right) \quad (48)$$

CHAPTER 3

NUMERICAL ANALYSIS OF SOLAR CHIMNEY POWER PLANT

In this part of the thesis, verification study is presented, for this purpose mesh independency study is performed and validation with an experiment study from the literature is performed. After reaching satisfactory results that are consistent with the literature the effect divergence chimney on the performance is investigated.

3.1. Pre-Processing

The schematic view and parameters of the chimney is shown in Figure 3.1. The dimensions for solar divergent chimney power plant is 350 cm chimney high (H_{CH}), 35 cm chimney exit (D_U), 25 cm chimney inlet (D_L), 6 cm collector height (H_C) and 400 cm (D_C) of collector diameter. Mesh independency study is performed for the divergent chimney with the given dimensions. The geometry is created with using ANSYS Geometry software.

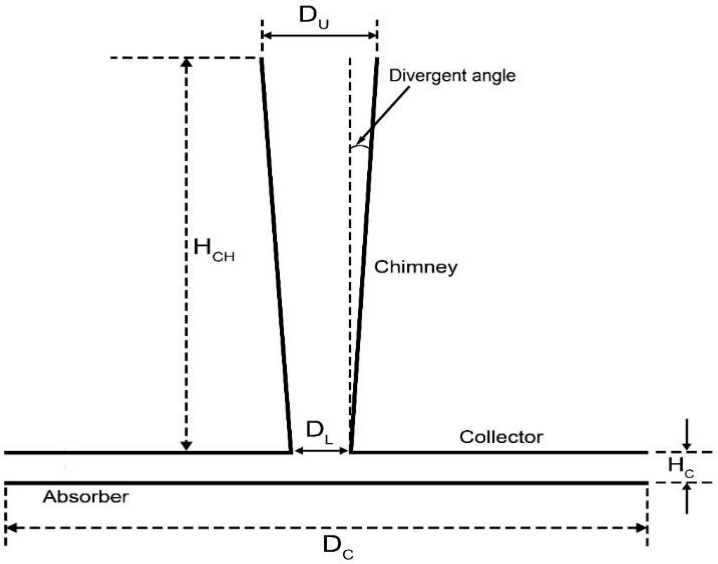

Figure 3.1: Parametric view of the SCPP

3.1.1. Boundary Conditions

The Boussinesq approximation is used to model the buoyancy flow. For the collector ceiling semi-transparent wall is used. The solar radiation (G) varies for each hour. The absorber emissivity is 0.55 and collector glass emissivity is 0.9. The pressure operation for Ankara is 90000 Pa. Furthermore, the ambient temperature (T_a) value is varied for every hour obtained from the Meteorological serves. Table 3.1 show the boundary condition for the SCPP. Figure 3.2 describes the boundary condition for the solar divergent chimney power plant.

Table 3.1 Boundary conditions

Surface	Type	Value
Collector inlet	Pressure inlet	P_i = 0 Pa, T=T_a
Absorber	Heat flux Wall	G = variable value
Chimney wall	Adiabatic wall	q= 0 W/m^2
Collector	Wall	T_a= variable value h = 5 W/m^2K
Exit of Chimney	Pressure outlet	P_o = 0 Pa

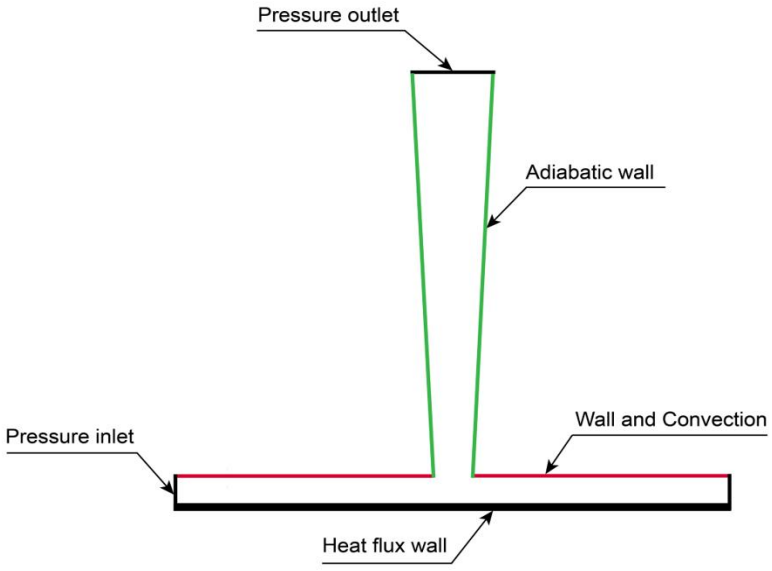

Figure 3.2: The boundary conditions for SCPP.

3.1.2 Meshing

To analyze the performance of the divergence chimney power plant, 2-D geometry model of divergence chimney is prepared. The system consists of three parts as absorber layer, divergence chimney, and collector. ANSYS Meshing software is used for meshing the solar chimney. The tetrahedral mesh elements are used in the computational domain. Figure 3.3 illustrates the meshing structure. To obtain more accurate results, mesh is refined near the chimney wall, at the chimney outlet and in the turbine location.

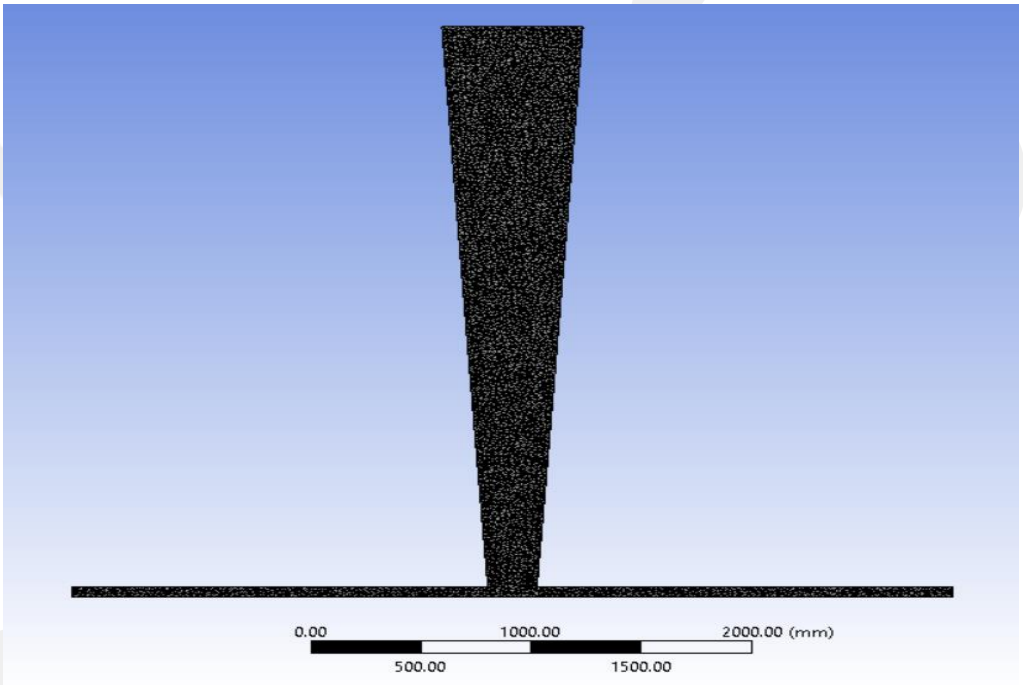

Figure 3.3. The meshing structure for divergence chimney

3.1.2.1. Mesh Independency

A mesh independency test is conducted to determine the proper number of cell which gives mesh-independent results. For this purpose, four different mesh structures are prepared with tetrahedral mesh elements. In Figure 3.4, temperature change for different number of meshes are shown. According to the results, after 10^6 mesh element results become independent from the mesh. Therefore, with also considering computational time one million elements are chosen.

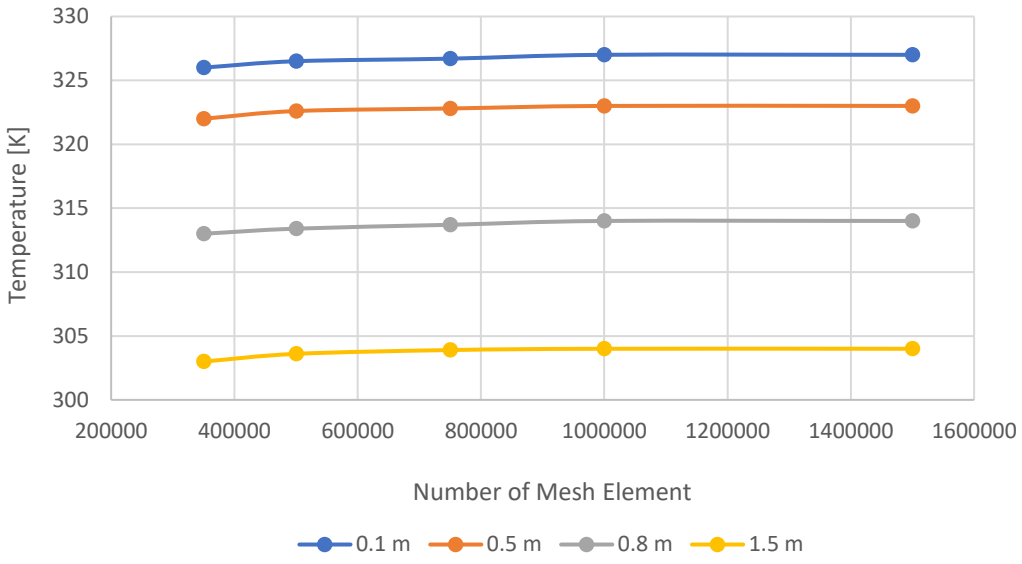

Figure 3.4: Mesh independency study

3.2. Model Verification

Numerical analysis is performed using ANSYS Fluent Software [65] for incompressible, two-dimensional, steady-state conditions. The convection terminology values can be obtained by using UPWIND second-order exact differencing rely on the SIMPLE method. The SCPP geometry is prepared with ANSYS Geometry module, then meshing operations are performed with using ANSYS Meshing tool. Results are examined with the help of temperature contours, pressure contours and velocity streamlines. Also, efficiency and power values are calculated with using the theoretical formulations that are given in Chapter 2. The model verification is accomplished using the experimental results of Ghalamachi et al. [56]. The operating conditions of the experiment is given in Table 3.2.

Table 3.2. Operating conditions and geometrical parameters of the experiment [56].

Parameter	**Value**
Chimney radius	10 cm
Collector radius	150 cm
Collector height	6 cm
Chimney height	300 cm
Solar Radiation	850 W/m^2
Average ambient temperature	302 K

According to the obtained CFD results, temperature distribution and velocity distribution through the chimney are compared with the experimental data. In Table 3.3, RMSE errors for numerical velocity values are shown. Relative mean errors are less than 6.4% for the temperature and 4.5% for the velocity distributions.

Table 3.3. Experimental and numerical velocity values at different collector locations

Collector Radius (m)	**Velocity Obtained from Exp [52] (m/s)**	**Velocity Obtained from Numerical (m/s)**	**Error %**
0.1	1.53	1.52	0.70
0.23	0.68	0.63	7.98
0.46	0.33	0.32	3.26
0.54	0.29	0.28	4.21
0.65	0.22	0.21	5.86
0.72	0.20	0.22	5.93
0.84	0.18	0.21	5.00
0.92	0.14	0.19	5.70
1.02	0.13	0.15	5.08
1.11	0.14	0.13	3.80
1.21	0.14	0.14	1.92
1.39	0.14	0.14	2.50
1.44	0.12	0.11	4.67
1.50	0.12	0.12	2.27

3.3 Effect of divergence angle of divergent chimney on SCCP performance

In this part the effect of chimney divergence angle on the performance of solar chimney power plant and power output is investigated. The inlet diameter for the chimney divergent is fixed (25 cm) and the outlet diameter is changed between $25 < D_U < 73.94$. The outlet diameter depends on the chimney angle variation. In Figure

3.1 divergence angle and Du is depicted. Table 3.4 shows detailed information about divergence angle and Du (cm) that are used in order to make parametric study.

Table 3.4: Configurations of SCPPs used in the parametric study

Case	**α (Inclination Angle)**	**D_u (Cm)**
1	0	25
2	0.3	28.6
3	0.8	35
4	1	37.21
5	1.5	43.32
6	2	49.44
7	3	61.68
8	4	73.94

In Figure 3.5, normalized power versus inclination angle is shown for different inclination angles of the diverging chimney. As can be concluded from the figure, up to a critical inclination angle, increasing the angle rises the output power. About 3º of inclination angle, peak power is 2.18 times the benchmark case (case 1). After reaching peak power value, power decreases with increasing the inclination angle further because of the outlet diameter increases which affect the air velocity and the buoyancy force have low impact at the exit point.

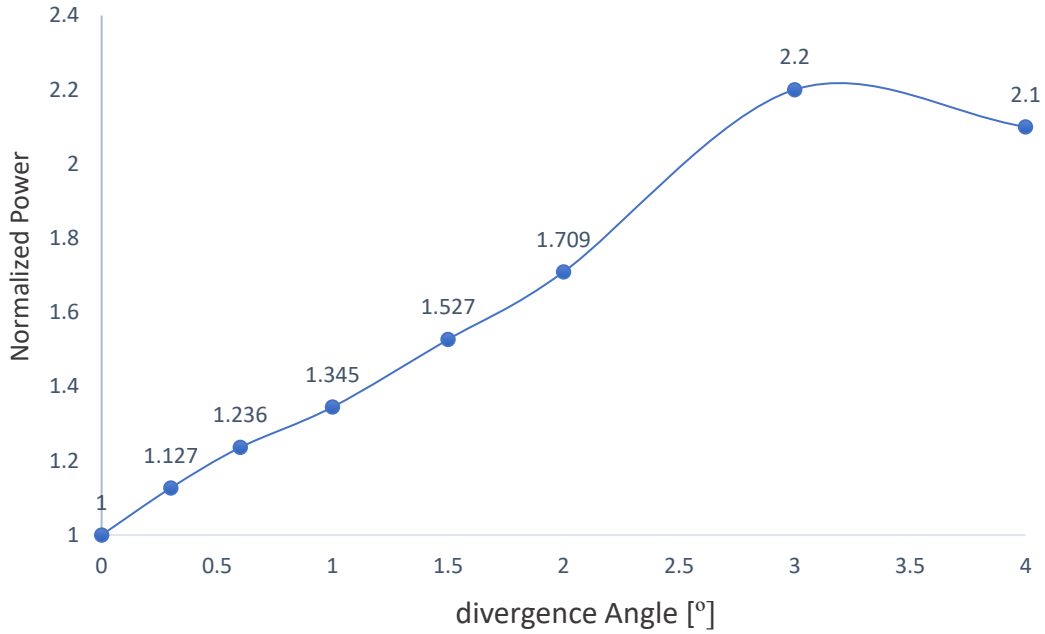

Figure 3.5: Normalized power output values for different inclination (divergence)

On the other hand, when case 8 is compared with case 7, dissipation is very large in case 8, which causes a reduction in the power output. Although when compared with the other inclination angles of diverging chimney, power is reduced in case 8. Case 8 still provides more power and is more efficient than straight chimney geometry. Further increase of the inclination angle results in more power decrease and also some constructional problems since the top diameter of the chimney gets very high.

CHAPTER 4

EFFECT OF DAILY SOLAR RADIATION AND DIFFERENT TEMPERATURES ON SCPP PERFORMANCE IN DIFFERENT MONTHS

4.1 Introduction

In this part, after obtaining the best design for the solar chimney model with a 3.5 m. chimney height, 4 m. collector diameter, 0.06 m. collector height, 0.25 m. inlet chimney diameter, and a 0.6168 m. outlet chimney diameter, the amount of solar radiation and weather temperature were analyzed and the effects of the irradiance and air temperature on the output power of the SCPP were studied during the period (17 January, 15 April, 17 July and 15 October in 2018). The temperature, pressure and velocity distributions inside the solar collector were determined daily.

The feasibility of solar chimney power plants in Ankara, Turkey is analyzed with the developed methodology. For this purpose a Matlab code is developed which calculates the solar irradiance values. With using the data that is obtained from the Matlab, numerical analysis is conducted with using ANSYS Fluent. Also ambient temperature values (meteorological data) is used in the numerical analysis. The flow chart of this part of the research is shown in Figure 4.1.

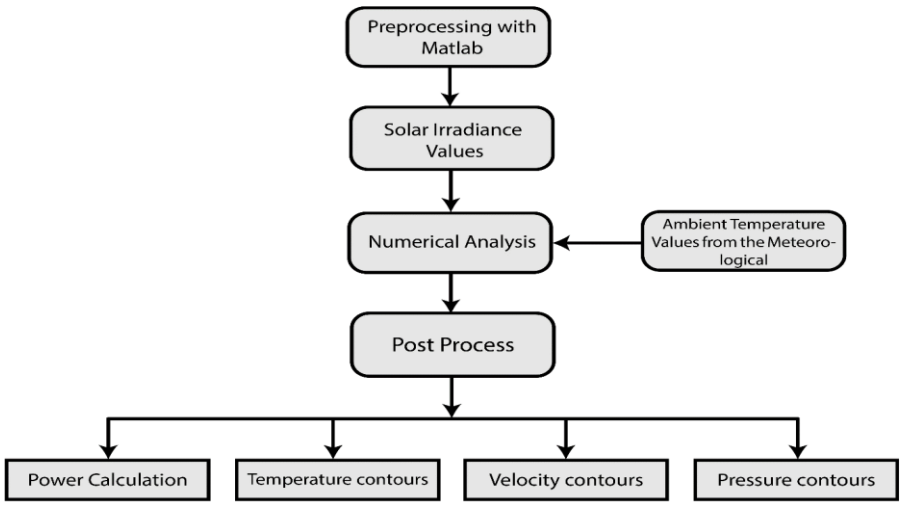

Figure 4.1: Solar Radiation Calculation with developed Matlab Code

4.2. Solar Irradiation Calculation with using Lui-Jordan Equations

After obtaining the best values for the dimensions of the solar chimney power plant, the values of total solar radiation are obtained for each hour and for four days per year (17 January, 15 April, 17 July and 15 October in 2018) with using Matlab software. The code was implemented based on the equations mentioned in the second chapter for the solar energy equations. Variable values were entered for each hour and for each day in the code, and then the total solar radiation value for each hour was obtained based on inputs which are latitude for Ankara, Monthly average daily total radiation on the terrestrial horizontal surface (H), Monthly average total radiation on the extraterrestrial horizontal surface (H_O) and Number of day (N) as shown in Figure 4.2.

The Tables 4.1, 4.2, 4.3, 4.4 show the total solar radiation values for each hour and for four days per year (17 January, 15 April, 17 July and 15 October in 2018) that is obtained with the help of the developed Matlab code. After obtaining the total solar radiation values, the value of total solar radiation (G), as mentioned in the boundary conditions in Table 3.1, for each hour is used in numerical analysis in order to obtain the power values.

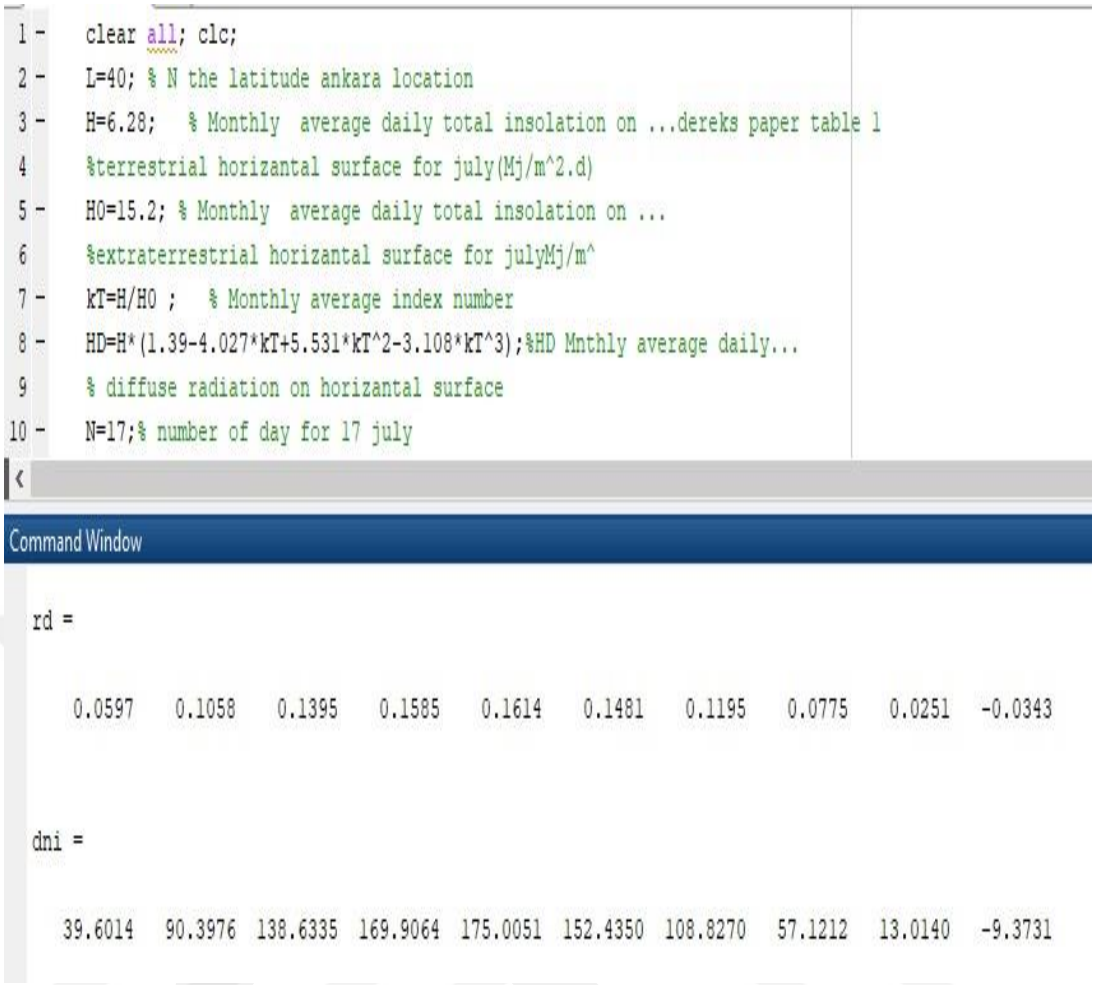

```
clear all; clc;
L=40; % N the latitude ankara location
H=6.28;   % Monthly  average daily total insolation on ...dereks paper table 1
%terrestrial horizantal surface for july(Mj/m^2.d)
H0=15.2; % Monthly  average daily total insolation on ...
%extraterrestrial horizantal surface for julyMj/m^
kT=H/H0 ;   % Monthly average index number
HD=H*(1.39-4.027*kT+5.531*kT^2-3.108*kT^3);%HD Mnthly average daily...
% diffuse radiation on horizantal surface
N=17;% number of day for 17 july
```

Command Window

```
rd =

    0.0597    0.1058    0.1395    0.1585    0.1614    0.1481    0.1195    0.0775    0.0251   -0.0343


dni =

   39.6014   90.3976  138.6335  169.9064  175.0051  152.4350  108.8270   57.1212   13.0140   -9.3731
```

Figure 4.2: Developed Matlab Code

This study is conducted in Ankara (Latitude = 40° N and Longitude =32.8° E) city to calculate the power for four different days and in different seasons. In the following tables total solar radiation and temperature values are shown for each hour of the day.

Table 4.1: The solar radiation and ambient temperature on 17 January 2018 in Ankara.

Daytime hours	**Total Solar Radiation W/m^2**	**Temperature C$^\circ$**
The sunrise at 08:07		
08:30	39.6	5.2
09:30	90.4	5.6
10:30	138.6	6.1
11:30	169.9	6.7
12:30	175	6.7
13:30	152.4	6.7
14:30	108.8	6.75
15:30	57.12	6.5
16:30	13	6.2
The sunset at 17:50		

For Spring season, number of days of April is taken as 90+15= 105, H = 17.30 MJ/m^2 day, H_o= 34.6MJ/m^2 day, SL = 30 ^{o}

Table 4.2 The solar radiation and ambient temperature on 15 April.2018.

Daytime hours	**Total Heat Solar Radiation W/m²**	**Temperature C°**
The Sunrise at 06:11		
06:30	53.4	15.5
07:30	128.9	16.6
08:30	217.1	17.6
09:30	303.6	18.5
10:30	372.8	19.9
11:30	411.5	21
12:30	412.2	21
13:30	374.7	21
14:30	306.3	21
15:30	220.2	19.9
16:30	131.8	18.4
17:30	55.7	16.7
The sunset at 19:27		

For summer season, number of days of July is taken as 17 +181= 198, H = 24.91 MJ/m^2 day, H_o= 40.6 MJ/m^2 day, SL = 30 ^{o}

Table 4.3: The solar radiation and ambient temperature on 17 July 2018.

Daytime hours	**Total Heat Solar Radiation W/m²**	**Temperature C°**
The Sunrise at 05:33		
06:30	132.3	20.5
07:30	241.3	23.3
08:30	359.1	24.8
09:30	470.4	25.2
10:30	558.5	26.3
11:30	609.3	26.8
12:30	614.6	27.7
13:30	573.2	28
14:30	492.3	28
15:30	384.7	27.3
16:30	266.9	26.9
17:30	154.9	26.2
18:30	61.3	25
The sunset at 20:18		

For autumn season, number of days of October is taken as 273+15= 288, H = 12.13MJ/m^2 day, H_o= 22.5MJ/m^2 day, SL = 30 ^{o}

Table 4.4 The solar radiation and ambient temperature on 15 October 2018.

Daytime hours	**Total Heat Solar Radiation W/m²**	**Temperature C°**
The Sunrise at 06:58		
07:30	78	19.45
08:30	165.4	20.8
09:30	253.3	22.6
10:30	321.3	23.4
11:30	354.2	23.9
12:30	343.7	24.5
13:30	292.7	24.2
14:30	212.9	23
15:30	122.8	21.4
16:30	42.4	19
The sunset at 18:10		

4.3 Daily Ambient Temperature and Solar Radiation Variation Analysis

The earth revolves around the sun for a period of 365 days and as a result, it creates four seasons through which temperature and global solar radiation values vary greatly. Moreover, the earth rotates over a period of 24 hours which results in night and day. For the study, a simple model was designed using the ANSYS 19 R2 software to simulate the power and velocity values with respect to seasonal and daily changes for Ankara. The temperature values for each hour were obtained from the Turkish state meteorological service and the solar radiation values were calculated using MATLAB code for each hour and for each season daily average. The fixed values are for the location of Ankara at latitude 40° N, local longitude 32.8° E and standard longitude 30° for Turkey. The variable values such as each month's monthly average daily total insolation 'H' (J/m^2.day) can be seen in Table 2.1 [44]. The heat flux value was used for the boundary condition for the ANSYS software and it was found by multiplying

the value of the solar radiation by the collector glass emissivity (0.9) In fact, the emissivity value relies on the type of material that used a roof layer.

4.3.1 Winter Season

On 17 January 2018, the number of daytime hours was 9.51. Sunrise occurred at 8:07, so the solar radiation analysis started at 8:30 using the MATLAB code. The variable values were entered in the code as H (6.28), H_O (15.2) in addition to the number of the day for this month. The results are shown in Table A1. The data shows the solar radiation increasing gradually from the early morning to the top value in the middle of the day after which it begins a decline. However, the irradiance at midday is low because of the Earth be situated further away from the sun during the winter. The temperature is a little and very close all the sunshine hours on this day as shown in Figure 4.3.

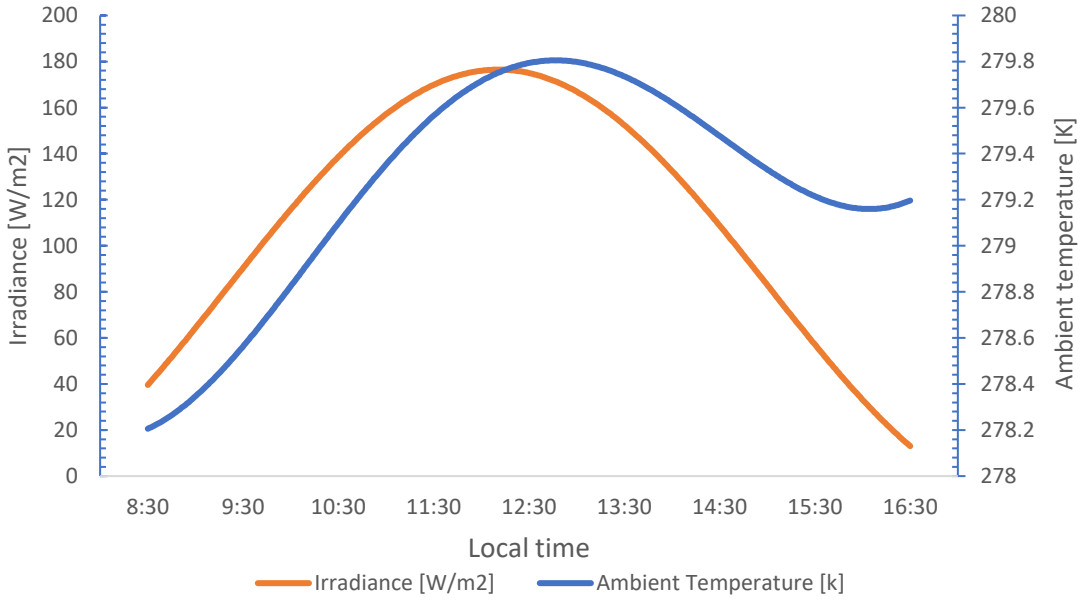

Figure 4.3: Ambient temperature and solar radiation distribution during the daytime for 17 January 2018.

4.3.2 Summer Season

The summer season has a greater amount of solar radiation reaching Ankara than other seasons. The MATLAB code shows that the variable values on 17 July were H (24.91) and H_O (40.6) and that the number of days was 181 + 17 = 198. The length of the

daytime was 14 hours 53 minutes. Sunrise occurred at 5:17 a.m. and sunset at 20:07 p.m. Table A2 shows the amount of solar radiation as being greater at midday for this day. The peak value occurred at 12:30 pm. due to the place of the sun at mid sky and vertical, so the sun's rays were short. Meanwhile the ambient temperature value peaked at 13:30 pm and remained the same until 14:30 pm, after which time it decreased gradually (see Figure 4.4). It can be noted in the figure that the top value ambient temperature did not occur at the same time as the solar radiation maximum.

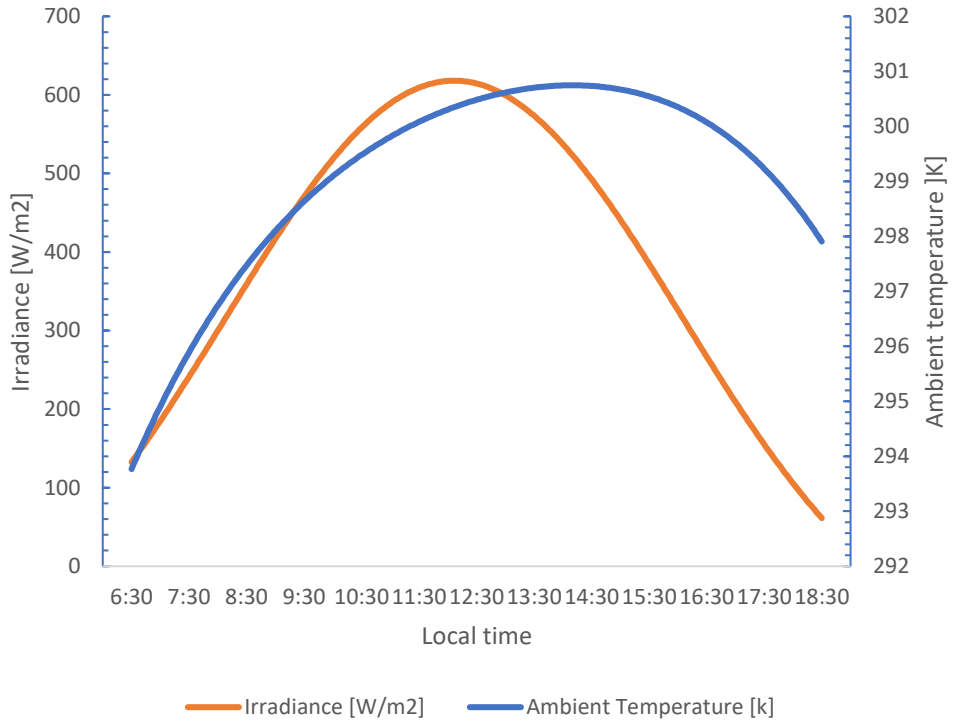

Figure 4.4: Ambient temperatures and solar radiation during the daytime on 17 July 2018.

4.3.3 Spring Season

The spring season is mild with daylight durations of 13.7 hours. The amount of solar radiation was obtained for each hour using MATLAB code. The variable values used in the code for 15 April were H (17:30) and H_O (34.6) and the number of days was 90 + 15 = 105 days, as shown in Table A3. Maximum solar radiation occurred at 12:30 pm and was almost equal at 11:30 am. Moreover, the amount of solar radiation after sunrise was almost equal prior to sunset, which shows that the solar altitude angle

is almost equal. The ambient temperature value reached a maximum at 11:30 am and remained at the same value until 14:30 solar radiation variation during the daytime is shown in Figure 4.5.

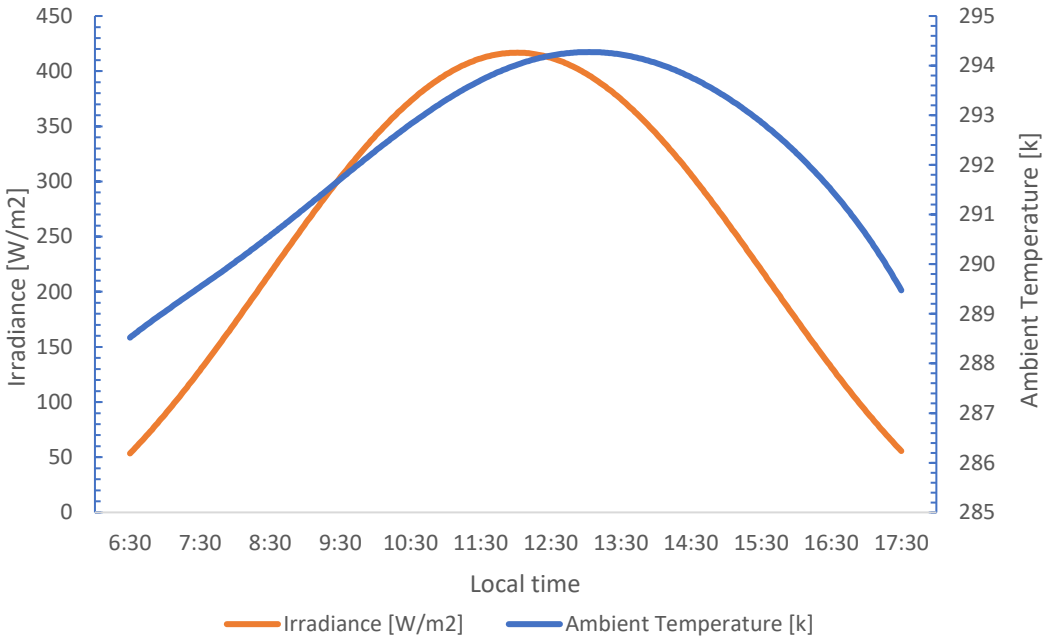

Figure 4.5: Ambient temperature values and solar radiation during the daytime on 15 April 2018.

4.3.4 Fall Season

The ambient temperature during the fall season in Ankara was mild, ranging from 19C to 25 C during the day on 15/10 according to meteorological statistics. The maximum ambient temperature reached 297.5 K at 12:30 pm, while the solar radiation peaked at 11:30 am after which time it dropped until the sunset, as shown in Figure 4.6. Sunrise occurred at 16:45, so the amount of solar radiation at 7:30 am was obtained using the MATLAB code. The variable values were entered into the code as H (12.13) and H_O (22.5) and the number of days as 273 + 15 = 288, as shown in Table A4.

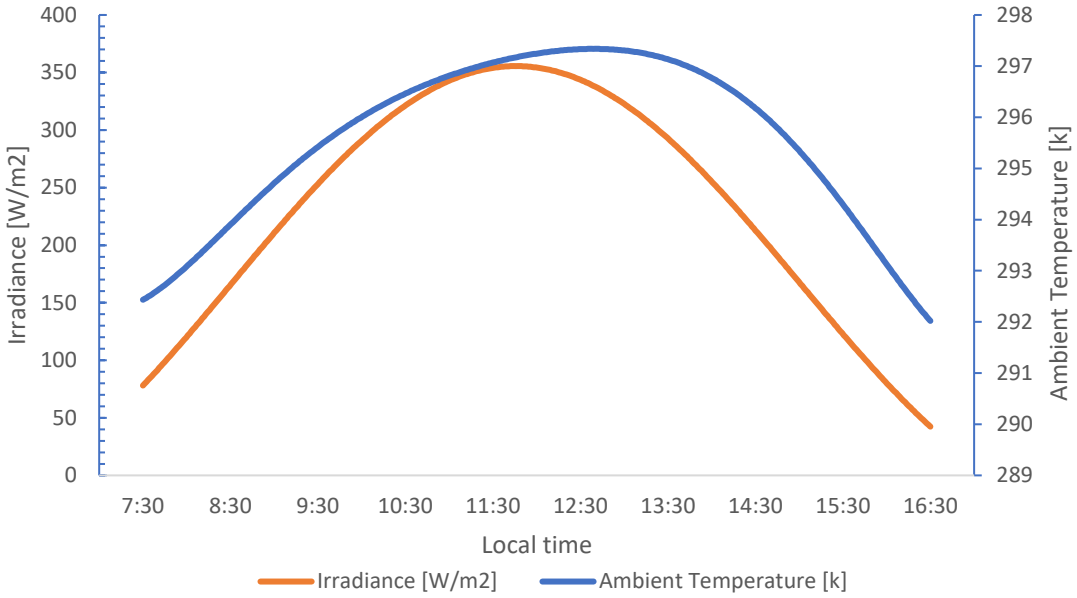

Figure 4.6: Ambient temperature values and solar radiation during the daytime on 15 October 2018.

4.4 Evaluation of the Effect of Ambient Conditions on SCPP Performance

Ambient temperature is considered to be the one of the factors that influences collector efficiency in a negative or positive manner. The surrounding temperature and its influence on performance and power are analyzed and studied. Solar irradiance is considered to be the most important factor that impacts SCPP performance such that the absorber layer absorbs the irradiance that is lost through the natural convection. This helps to increase the value of heat into the solar chimney. The investigation includes the study of the relationship between solar insulation and ambient temperatures during the daytime.

4.4.1 Effect of Ambient Conditions on Performance and Power during the Winter Season.

On 17 January 2018, three cases were selected: case (a) at 8.30 am; case (b) at 12:30 pm; and case (c) at 16:30 in the winter season. Figure 4.7 shows the air temperature distribution inside SCPP. The contours show the distribution of air temperature increasing gradually from the collector inlet until reaching the maximum value in the center of the collector as well as its heat intensity differing between the hours in the collector with it being hotter at 12:30 pm. It is notable that the collector inlet temperature is equal to the ambient temperature.

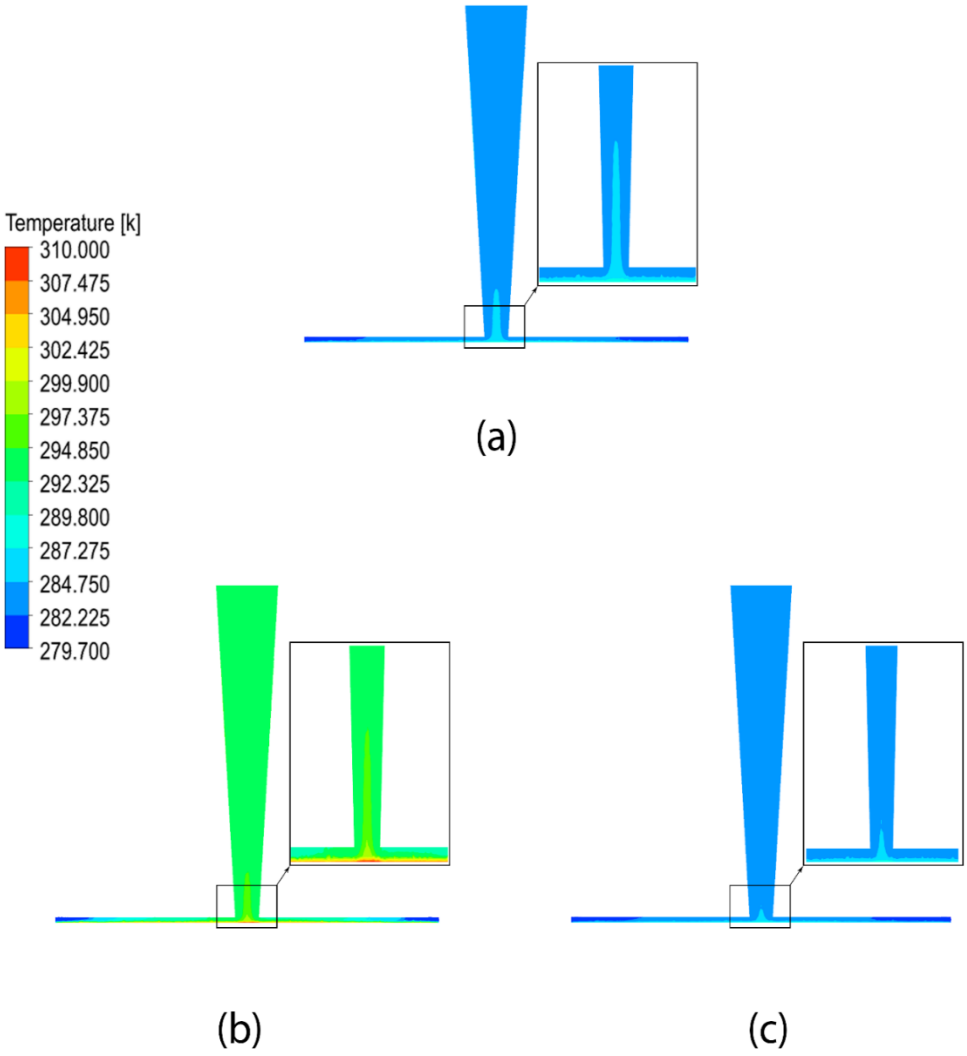

Figure 4.7: Simulation results for air temperature distributions for case (a) at 8:30, case (b) at 12:30 and case (c) at 16:30 for 17 January 2018.

The influence of the ambient temperature and irradiance on the air velocity distribution inside the SCCP are presented in Figure 4.8. The contours show that the maximum air velocity value in the inlet chimney was as indicated in the figure. The maximum of the air velocity value appears in case (b) at 12.30 when the maximum irradiance value was 175 W/m^2 and affected the output power value such that the output power reached its highest value on this day. The ambient temperature value was 279.7 K. After 12:30, the irradiance began to decrease and the air velocity value and output power decreased, while the ambient temperature continued to rise until 13.30 to 279.75 K. The air velocity value in case (a) was higher than that of case (c) Although the ambient

temperature value was lower, the amount of solar radiation is greater, as shown in Table 4.5.

Table 4.5: Air velocity values and output power during the daytime on 17 January 2018.

Time	Solar Radiation (W/m^2)	Velocity (m/s)	Temperature (K)	Power (kW)
8.30	39.6	0.53	284.2	0.04559
9.30	90.4	0.784	289.66	0.10859
10.30	138.6	0.847	293.58	0.16426
11.30	169.9	0.925	296.23	0.19805
12.30	175	0.941	296.57	0.20419
13.30	152.4	0.894	294.98	0.17601
14.30	108.8	0.799	291.72	0.12201
15.30	57.12	0.642	286.98	0.06028
16.30	13	0.439	281.58	0.010807

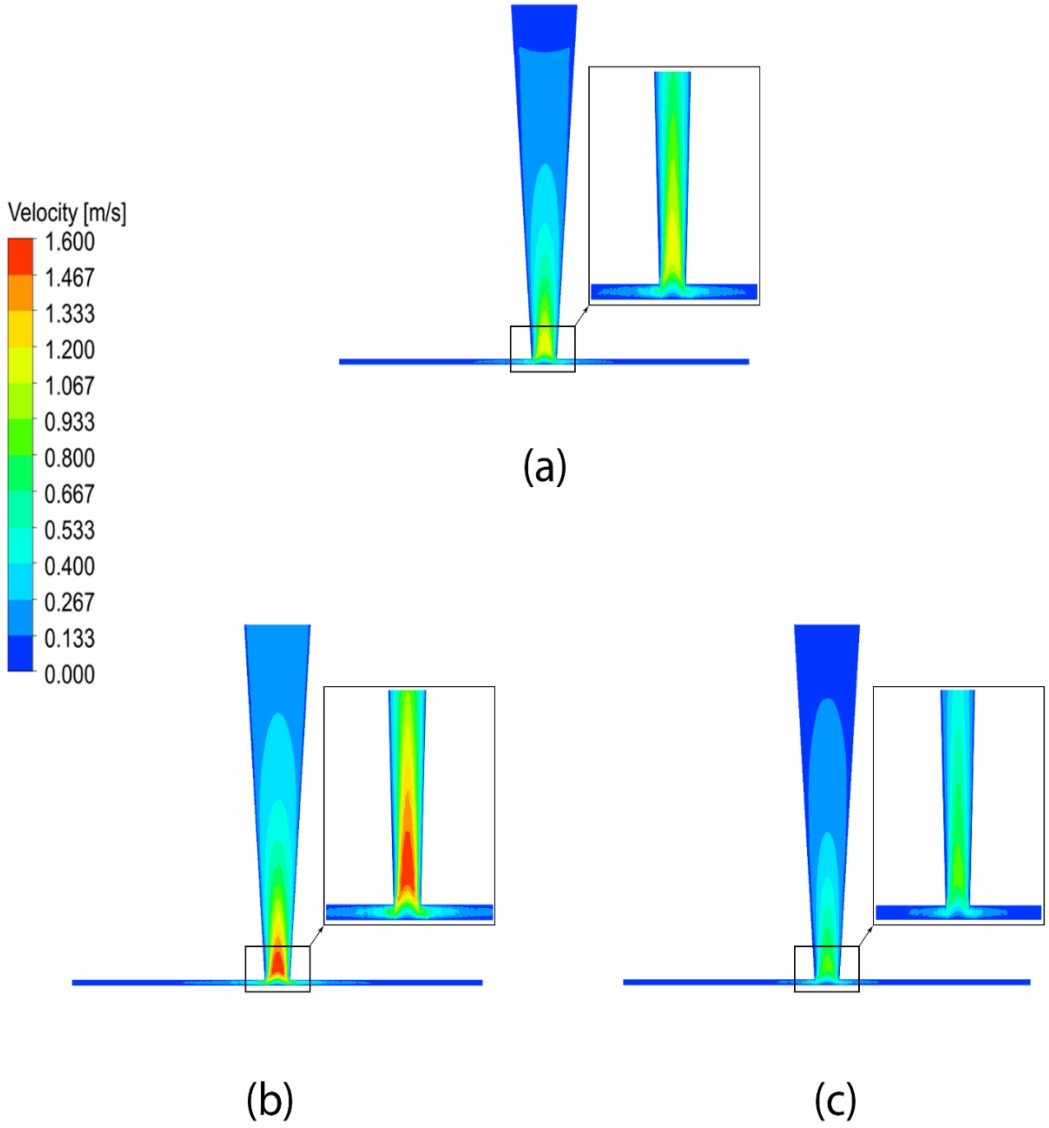

Figure 4.8: Simulation results for the distribution of velocities for case (a) at 8:30, case (b) at 12:30 and case (c) at 16:30 for 17 January 2018.

Figure 4.9 shows the effect of irradiance on the air velocity outlet. It can be observed that the air velocity rises with an increase in the ambient temperature. The results show the ambient temperature remaining constant between 11.30 and 12.30 while the irradiance value as well as the air velocity and output power continued to rise. The ambient temperature reached its peak at 13:30 while the solar radiation and the air velocity began to decrease thereby reducing the power output. The influences of varying the amount of solar radiation on the output power is illustrated in Figure 4.10.

It can be observed that there was an increase in the energy value that is directly proportional to the rise in solar radiation It is clear that solar radiation has an effect on the output power to a greater extent than does the ambient temperature.

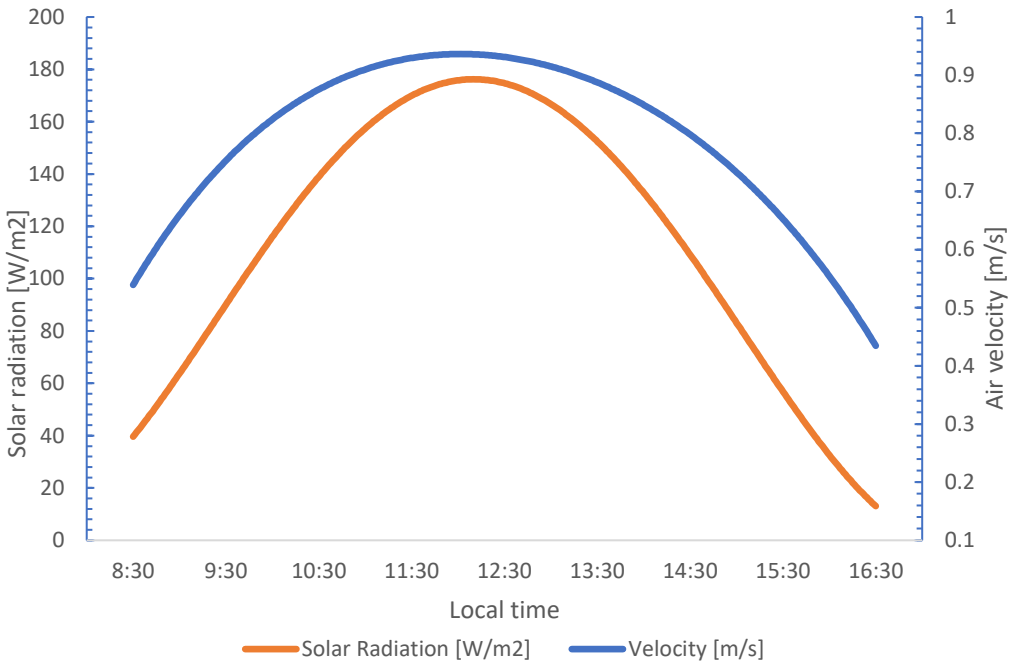

Figure 4.9: Air velocity values inside the SCPP with daily solar radiation during the daytime on 17 January 2018.

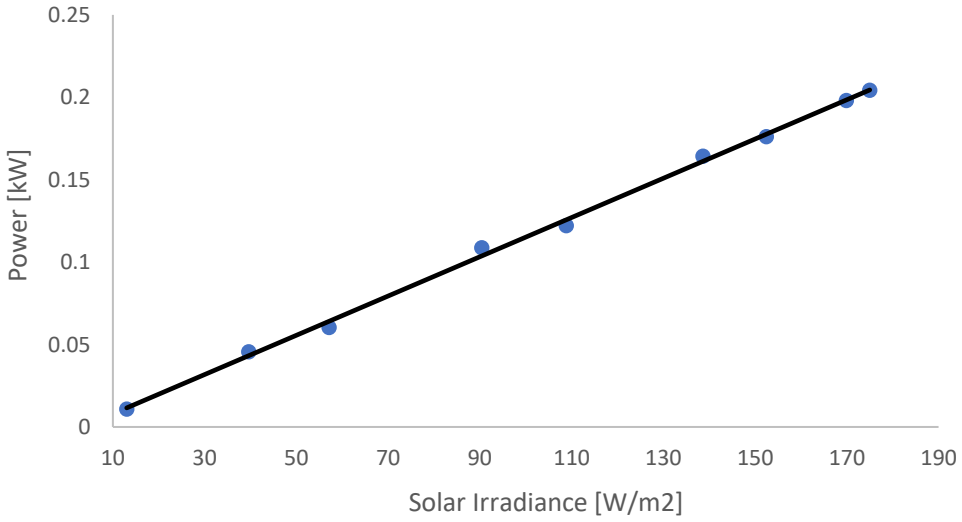

Figure 4.10: Relationship between solar irradiance and power output during the daytime on 17 January 2018.

The pressure difference is illustrated in Figure 4.11. The contours show the maximum pressure difference value is out of the collector and inlet of the chimney. In fact, when the pressure difference rose, it led to an increase in the air velocity value, which effectively increases the power. Case (b) at 12.30 pm had better results than case (a) and case (c) because irradiance was higher compared with other hours.

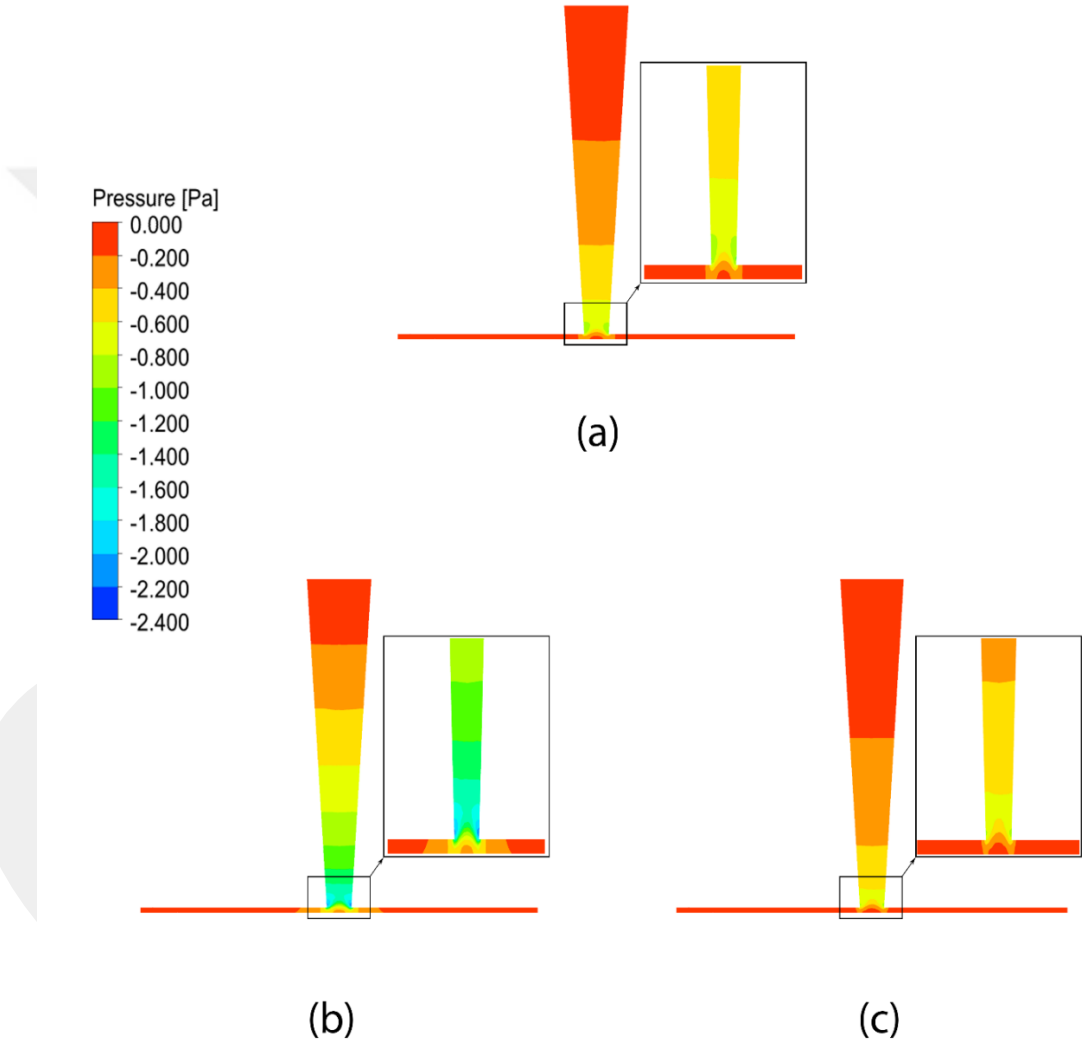

Figure 4.11: Simulation results for the static pressure distribution for case (a) at 8:30, case (b) at 12:30 and case (c) at 16:30 for 17 January 2018.

4.4.2 Effect of Ambient Conditions on Performance during the summer

The summer gave better results in terms of air velocity and output power because of the quantity of irradiance. The date of 17 July 2018 was selected with three cases: case (a) at 6:30, case (b) at 12.30 and case (c) at 18:30. Figure 4.12 illustrated the temperature of the air inside the SCPP. It can be observed that maximum hot air occurred at 12.30 with less severe hot air occurring at 18.30. Moreover, it can be noted that solar radiation a greater influence on hot air than the ambient temperature where the chimney outlet air temperature at 6.30 was higher than at 18.30, as shown in Table 4.6.

Table 4.6: Air velocity values and output power for 17 July 2018.

Time	Solar radiation (W/m^2)	Velocity (m/s)	Temperature (K)	Power (kW)
06:30	132.3	1.225	303.5	0.09095
07:30	241.3	1.445	312.12	0.18016
08:30	359.1	1.513	319.07	0.28018
09:30	470.4	1.617	324.33	0.38127
10:30	558.5	1.721	328.5	0.44958
11:30	609.3	1.763	331.6	0.48901
12:30	614.6	1.775	331.99	0.49041
13:30	573.2	1.725	330.6	0.45755
14:30	492.3	1.686	327.4	0.38539
15:30	384.7	1.615	322	0.28538
16:30	266.9	1.477	316.37	0.19022
17:30	154.9	1.414	309.56	0.09499
18:30	61.3	1.231	302.72	0.02925

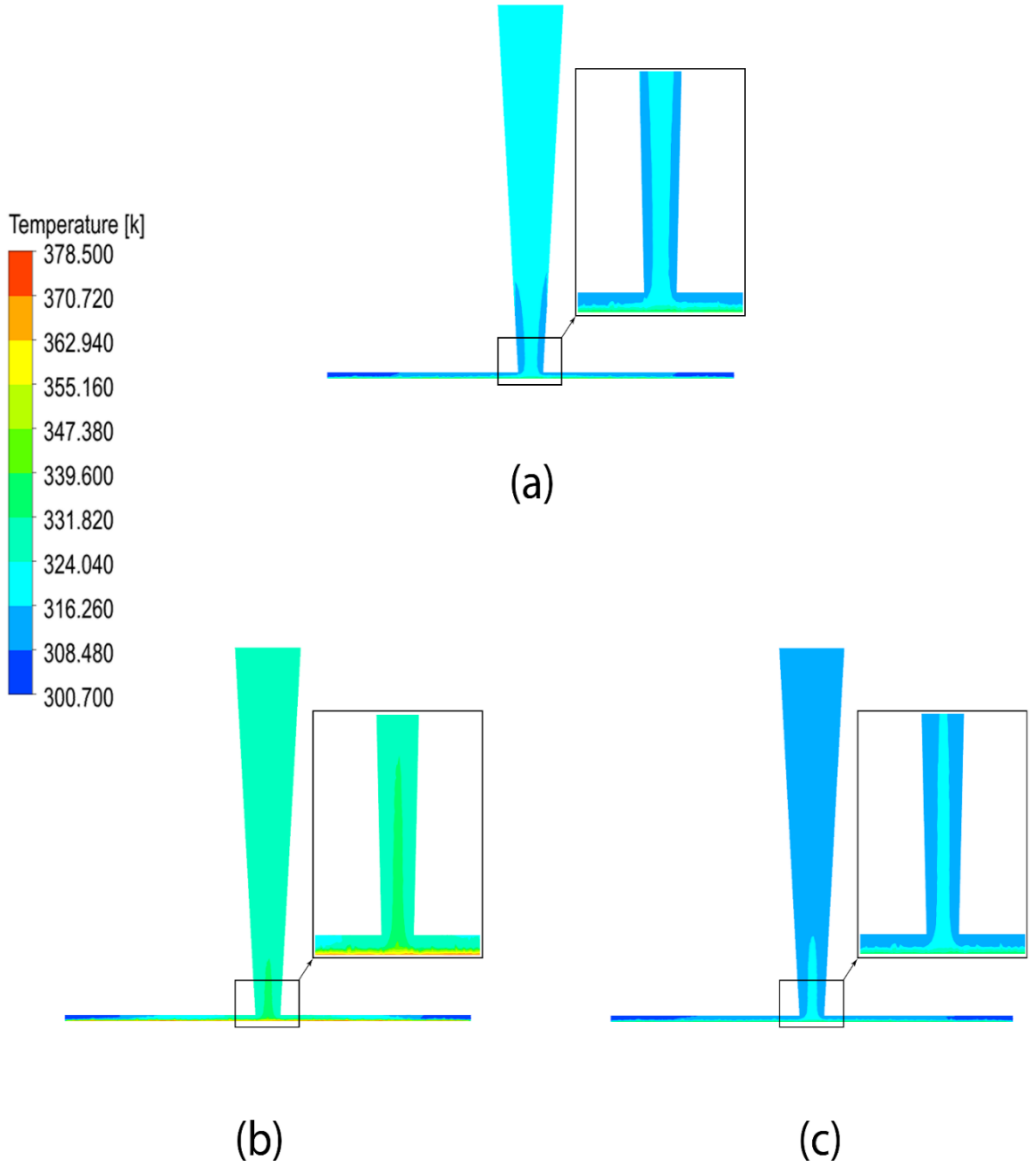

Figure 4.12: Simulation results for air temperature distribution for case (a) at 6:30, case (b) at 12:30 and case (c) at 18:30 for 17 July 2018.

The air velocity distribution inside the SCPP is illustrated in Figure 4.13. According to the findings, case (b) at 12:30 showed better results due to the high amount of solar radiation in the middle of the day. Case (c) at 18:30 showed better result than case (a) at 6:30 despite their having been a greater amount of solar radiation at 6:30 than at 18:30. This can be explained by the absorber layer being cold in the early morning and requiring time to be heated by irradiance; therefore, it absorbed the irradiance and ejected the heat by natural convection. However, in the final hour before sunset, the

absorber layer loses a huge heat amount, which leads to increases in the air velocity, as in case (c), despite the irradiance being low.

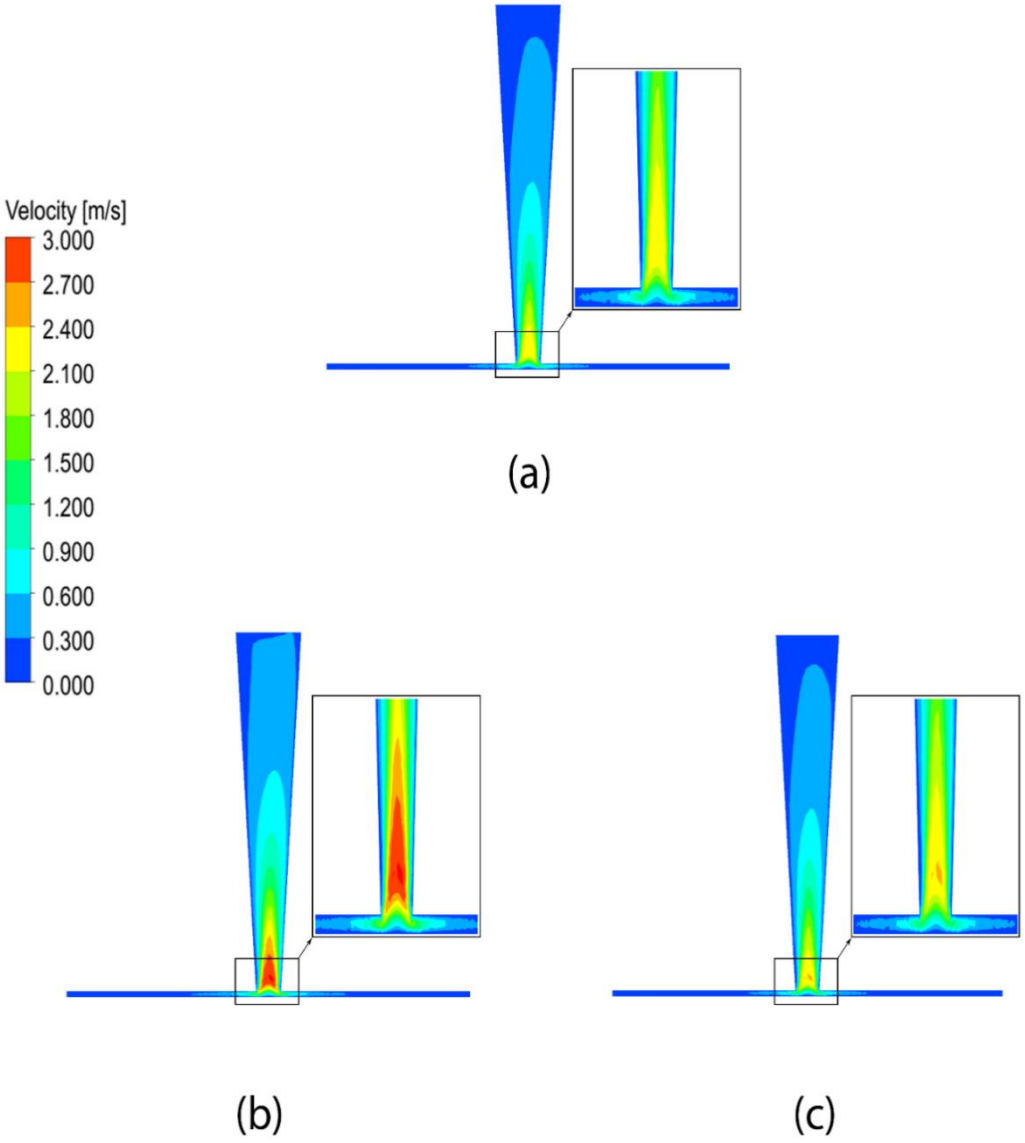

Figure 4.13: Simulation results for air velocity distribution for case (a) at 6:30, case (b) at 12:30 and case (c) at 18:30 for 17 July 2018.

The results show that the ambient temperature was 293.5 K at 6:30, the air velocity was 1.225 m/s and the power 0.09095 kW. The air velocity values reached their maximum point at 1.775 m/s with an output power value of 0.49041 kW at midday (12:30). The ambient temperature continued to rise until the peak period between

13:30 (301 k) and 14:30. The air velocity and output power values decrease with a decrease in the amount of solar radiation without the surrounding temperature affecting the air velocity and power. As shown in Table 4.6.

The impact of solar radiation during the day on the air velocity and output power is illustrated in Figure 4.14 and 4.15, respectively. It appears that the solar radiation increases during the morning until peak time at 12:30, at which time the air velocity had a high value. The outlet temperature was high so it had a positive effect on the amount of power with the irradiance intensity declining in the afternoon leading in turn to a reduction in the air velocity, and therefore, to a reduction in output power.

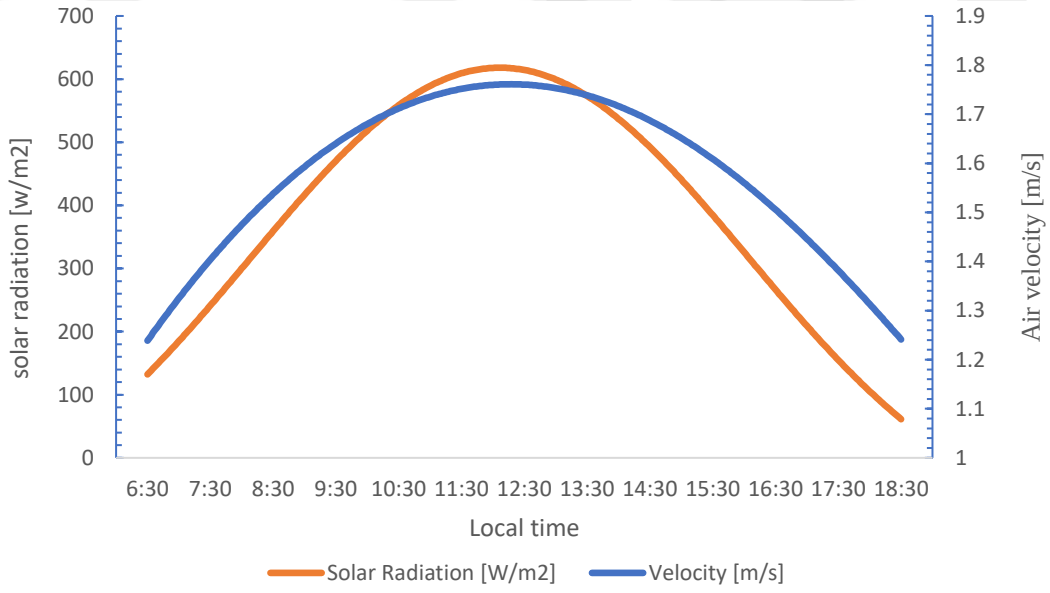

Figure 4.14: Variation of solar radiation with air velocity during the daytime on 17 July 2018.

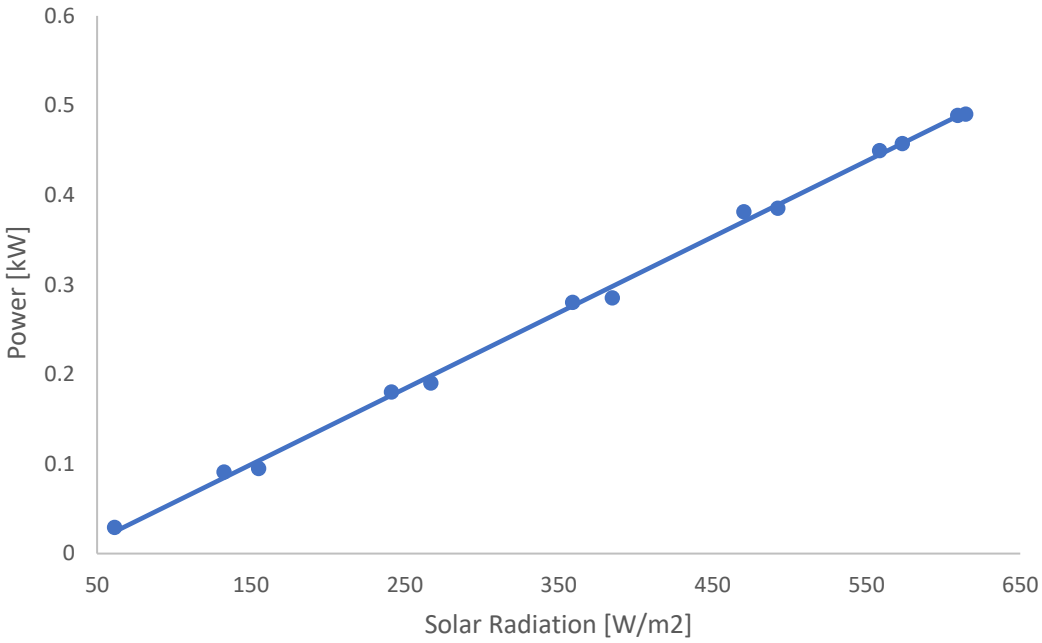

Figure 4.15: Variation of solar radiation with output power during the daytime on 17 July 2018.

When the solar radiation increased, the air temperature inside the SCPP and ground temperatures also increased, thereby leading to an increase in the pressure difference, leading in turn to an increase in air velocity. Case (b) produced a better result due to midday being the time of highest irradiance, as shown in Figure 4.16.

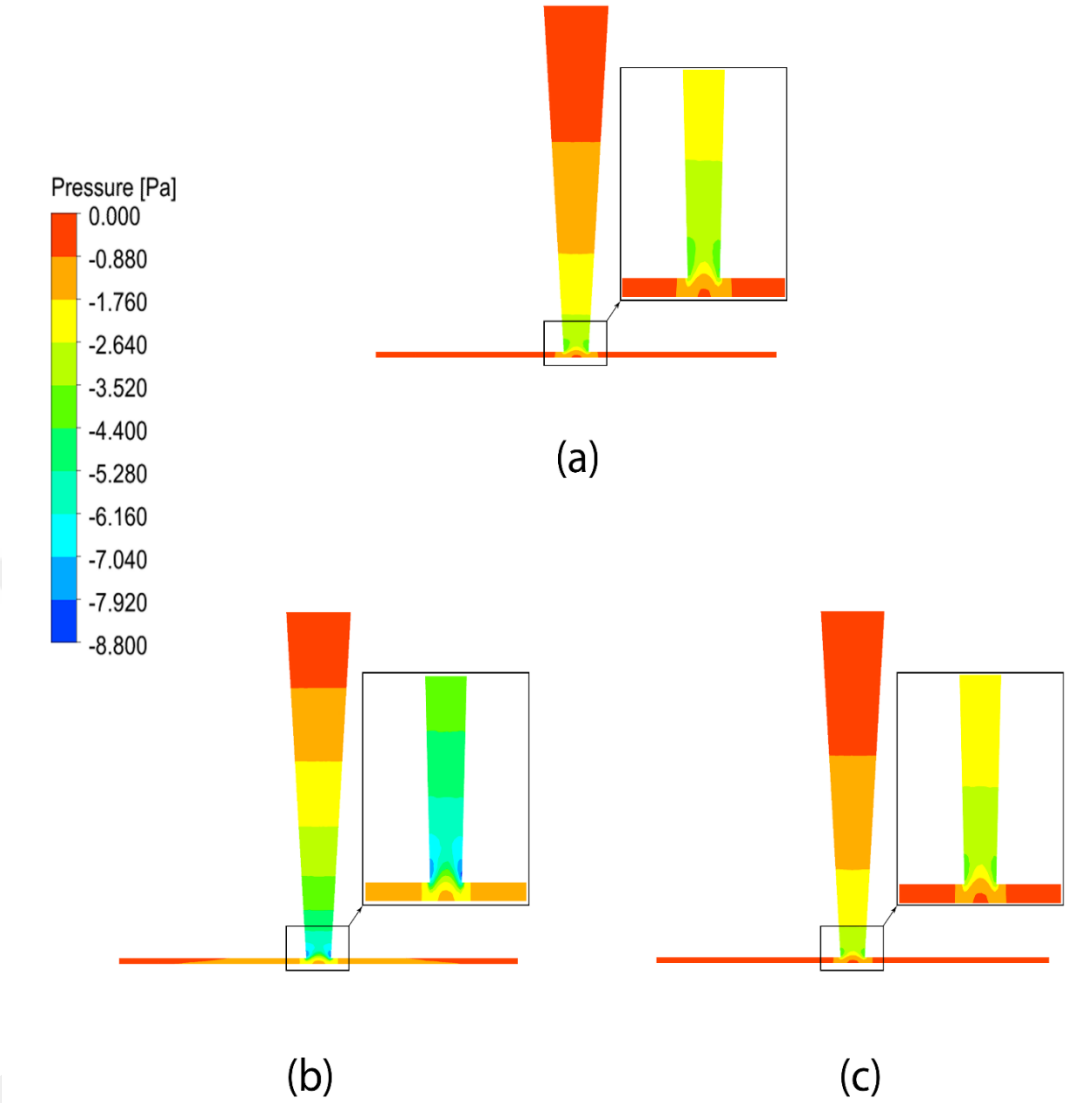

Figure 4.16: Simulation results for static pressure distribution for case (a) at 6:30, case (b) at 12:30 and case (c) at 18:30 on 17 July 2018.

4.4.3 Effect of Ambient Conditions on Performance during the Spring Season

During the spring on 15 April 2018, three cases were selected: case (a) at 6:30, case (b) at 12:30 and case (c) at 17:30. Figure 4.17 shows distribution of the air temperature inside the SCPP. The results, as expected, for case (b) were the best such that the intensity of the solar radiation increased, which remarkably affected the air temperature in the collector. The results for 11:30 are similar to those of 12:30 due to the level of solar radiation having been almost identical, as shown in Table 4.7.

Table 4.7: Air velocity values and output power for 15 April 2018.

Time	Solar radiation (W/m^2)	Velocity (m/s)	Power (kW)
06:30	53.4	0.989	0.03339
07:30	128.9	1.13	0.10134
08:30	217.1	1.22	0.18677
09:30	303.6	1.44	0.25821
10:30	372.8	1.51	0.31727
11:30	411.5	1.56	0.34861
12:30	412.2	1.561	0.34895
13:30	374.7	1.51	0.31296
14:30	306.3	1.45	0.23431
15:30	220.2	1.23	0.18603
16:30	131.8	1.115	0.08585
17.30	55.7	0.941	0.02762

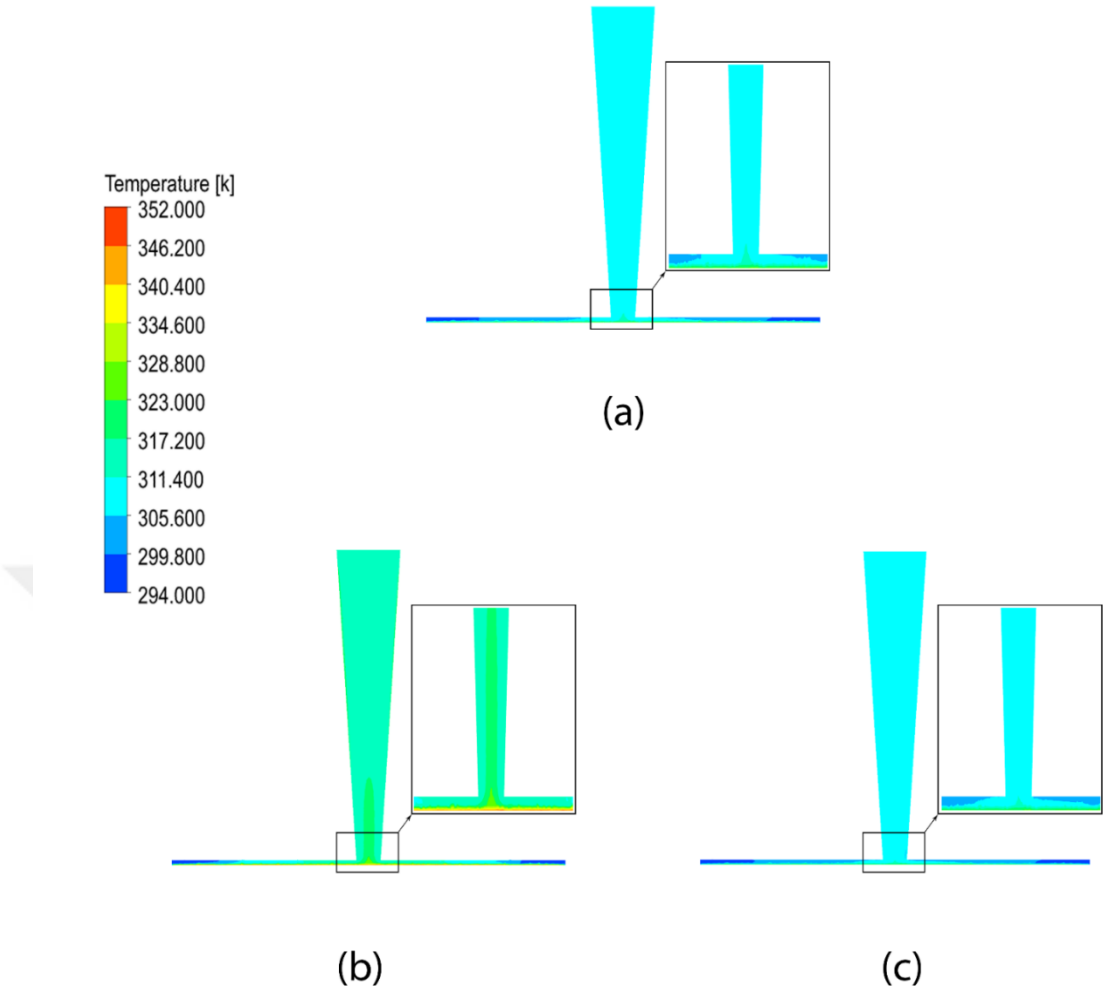

Figure 4.17: Simulation results for air temperature distribution for case (a) at 6:30, case (b) at 12:30 and case (c) at 17:30 for 15 April.

Although the ambient temperature is constant between 11:30 and 14:30 at approximately 294 K, the air velocity is variable and depends on the amount of solar radiation. The ambient temperature has no impact on the output power and it is notable that the ambient temperature rises since the morning with output power increasing. However, at 11:30, the ambient temperature remains constant for four hours with the amount of energy continuing to rise. The distribution of the air velocities based on the amount of solar radiation inside the SCPP during daytime contour is illustrated in Figure 4.18. According to the daily analyses, in case (b) at 12:30 pm, the maximum air velocity distribution appears in midday due to it has a great amount of irradiance that affects the collector layer. The results show that case (a) is better than case (c)

despite the amount of irradiance in the early morning at 6:30 being lower than at 17:30. It is indicated that the ambient temperature has a negative effect on the air velocity and output power. The ambient temperature at 6:30 is 288.5 K and at 17:30, it is 289.5 K. When the ambient temperature is high, it leads to the density of the air inside the SCPP being reduced, thus the air velocity decreases because of the principal buoyant force which depends on the difference of temperature between the air temperature inlet and air temperature outlet. A greater difference in the temperature always gives better results. The influence of the amount of solar radiation on the air velocity is illustrated in Figure 4.19. According to the results, increases and decreases in solar radiation cause a significant change in the air velocity value.

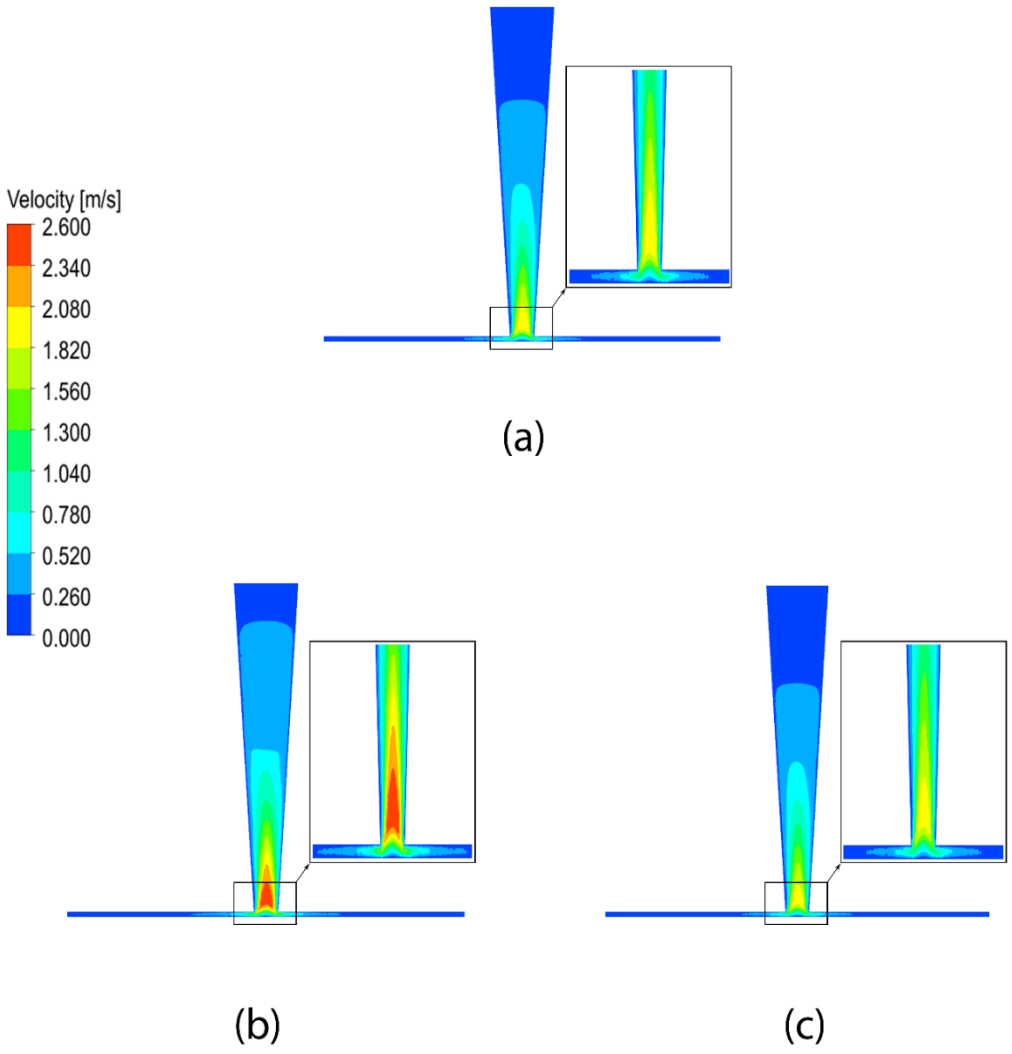

Figure 4.18: Simulation results for air velocity distribution for case (a) at 6:30, case (b) at 12:30 and case (c) at 17:30 on 15 April 2018.

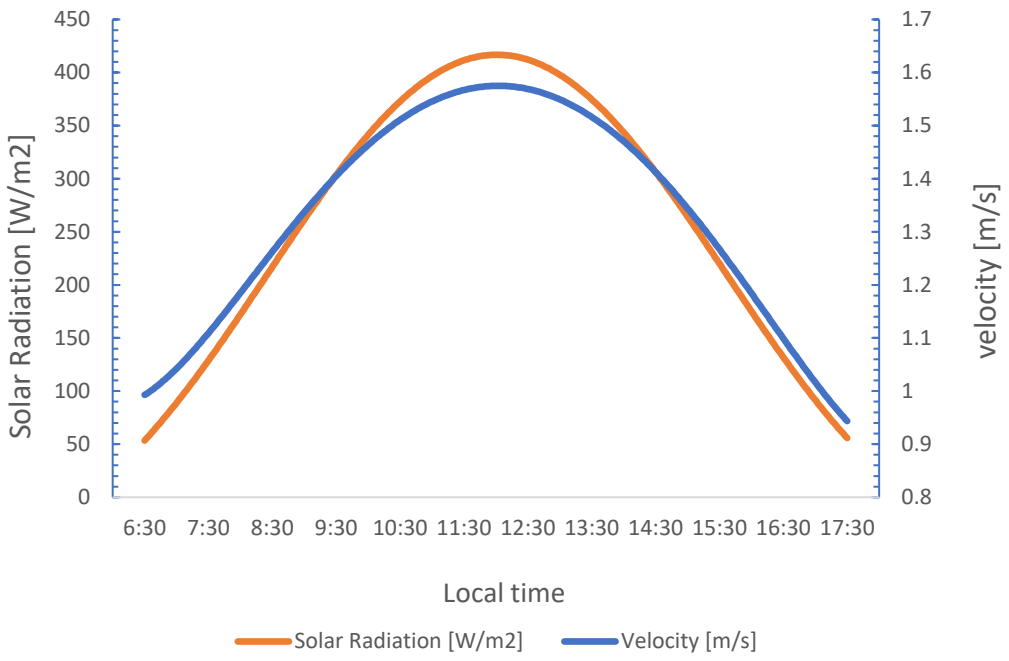

Figure 4.19: Variation of solar radiation with air velocity during the daytime on 15 April 2018.

The effect of changing the amount of solar radiation on the output power of the SCPP during the spring season is illustrated in Figure 4.20. According to these results, when the solar irradiance rose, the output power increased; however, from the figure, it can be seen that there was drop. In fact, this temperature difference effect occurred during the daytime.

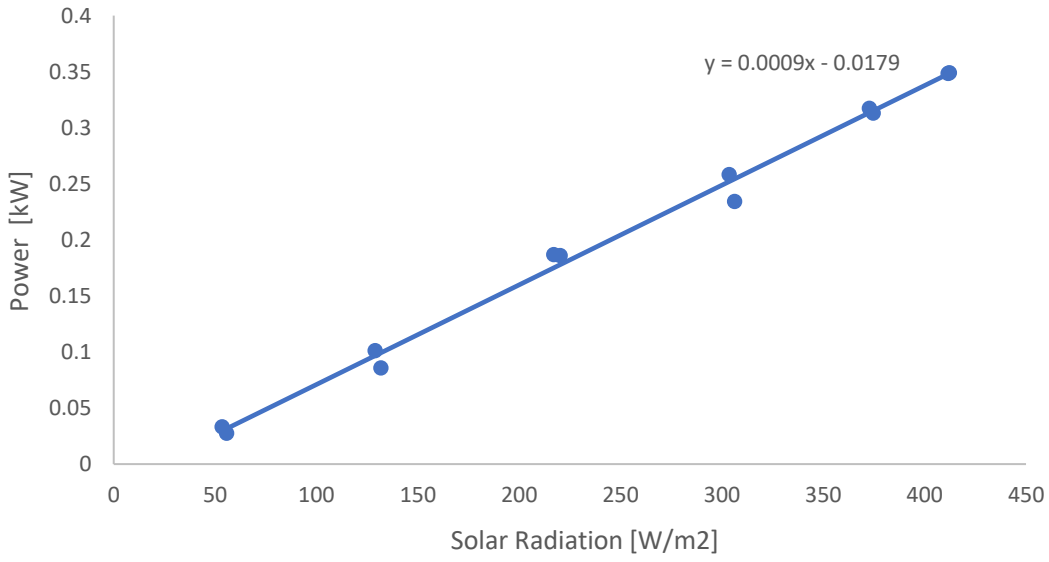

Figure 4.20: Variation of solar radiation with the output power on 15 April 2018.

The impact of varying weather conditions through irradiance intensity and ambient temperature on flow pressure is illustrated in Figure 4.21. According to the results, case (b) had better pressure distribution at the inlet chimney which affected the air velocity. Therefore, case (b) had a large air velocity value.

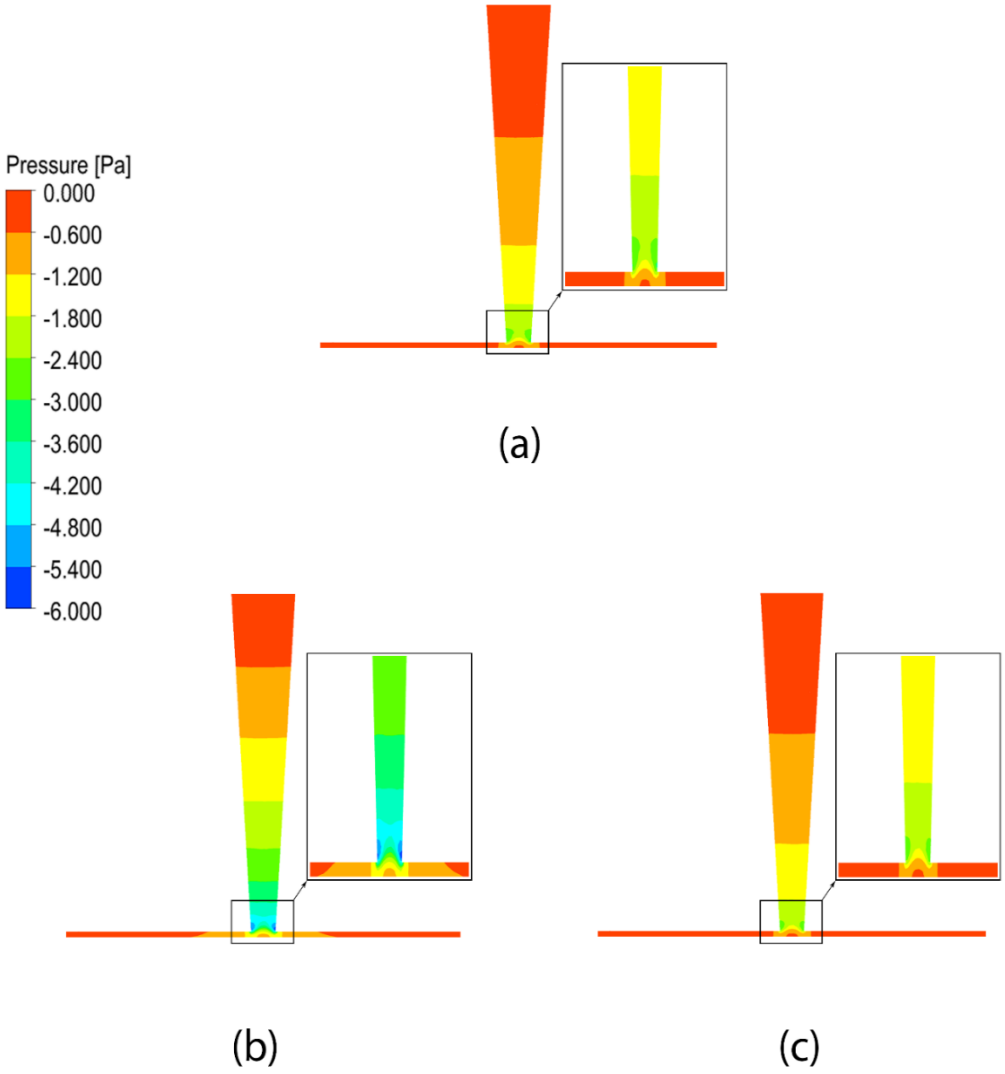

Figure 4.21: Simulation results for the static pressure distribution for case (a) at 6:30, case (b) at 12:30 and case (c) at 17:30 for 15 April 2018.

4.4.4 Effect of Ambient Conditions on Performance during the Fall Season

For the fall season on 15 October 2018, three cases were selected to describe the influence of the environmental conditions on the air velocity and output power during the daytime, namely case (a) at 7:30, case (b) at 11:30 instead 12:30 (due to a greater amount of solar radiation) and case (c) at 16:30. In Figure 4.22, it is notable that case (b) has a good distribution of air temperature inside the SCPP due to the level of irradiance and high temperature difference. In Table 4.8, the results show air velocity and output power for each hour beginning after sunrise and lasting until the final hour of daylight.

Table 4.8: Air velocity values and output power during the daytime on 15 October2018.

Time	Solar radiation (W/m^2)	Velocity (m/s)	Power (kW)
07:30	78	1.104	0.04718
08:30	165.4	1.351	0.11936
09:30	253.3	1.44	0.19353
10:30	321.3	1.523	0.25166
11:30	354.2	1.54	0.27922
12:30	343.7	1.538	0.26835
13:30	292.7	1.461	0.22308
14:30	212.9	1.431	0.15555
15:30	122.8	1.224	0.08105
16:30	42.4	1.036	0.02125

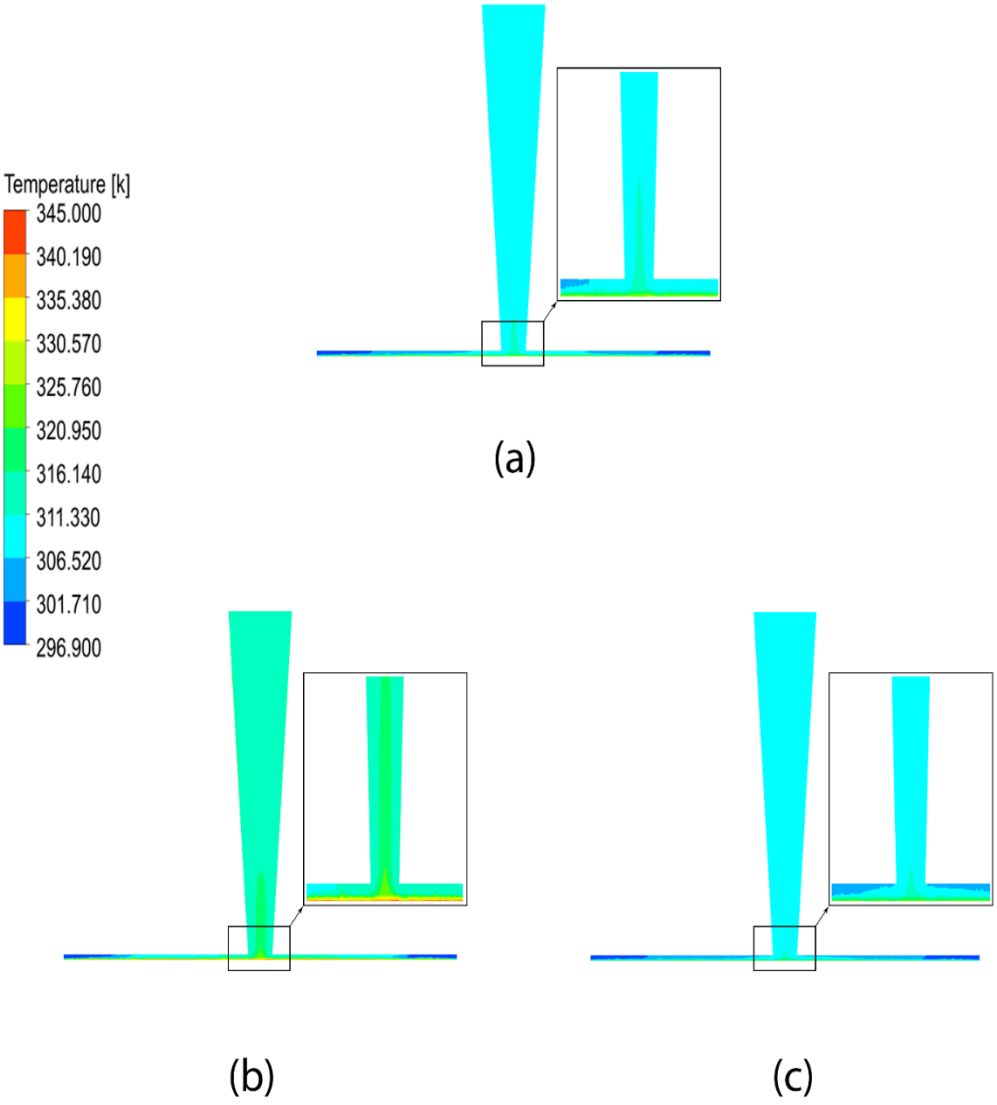

Figure 4.22: Simulation results for the air temperature distribution for case (a) at 7:30, case (b) at 11:30 and case (c) at 16:30 for 15 October 2018.

The impact of the change in the ambient temperature on the air velocity and power is presented in Figure 4.24 and Figure 4.25, respectively. The results indicate that the air velocity reached the peak point at 11:30 at 1.54 m/s and an ambient temperature of 296.9 K, while the ambient temperature continued to rise at 12:30 to a temperature of 297.5 K with an air velocity 1.538 m/s. Moreover, it was noted that the ambient temperature at 13:30 was higher than at 11:30 with the air velocity being the lowest. For the surrounding temperature influence on the output power, it was found that the power at 11:30 was higher despite the ambient temperature not having reached the peak time. Furthermore, when the ambient temperature rose the output power

decreased. Figure 4.23 illustrates the air velocity distribution contours based on the varying amounts of irradiance during the daytime. It is clear that case (b) at 11:30 had a great amount of irradiance, which had a significant effect on airflow velocity. Case (a) at 7:30 had a higher airflow value than case (c) at 16:30 and the outlet air temperature was higher despite case (a) in the early morning.

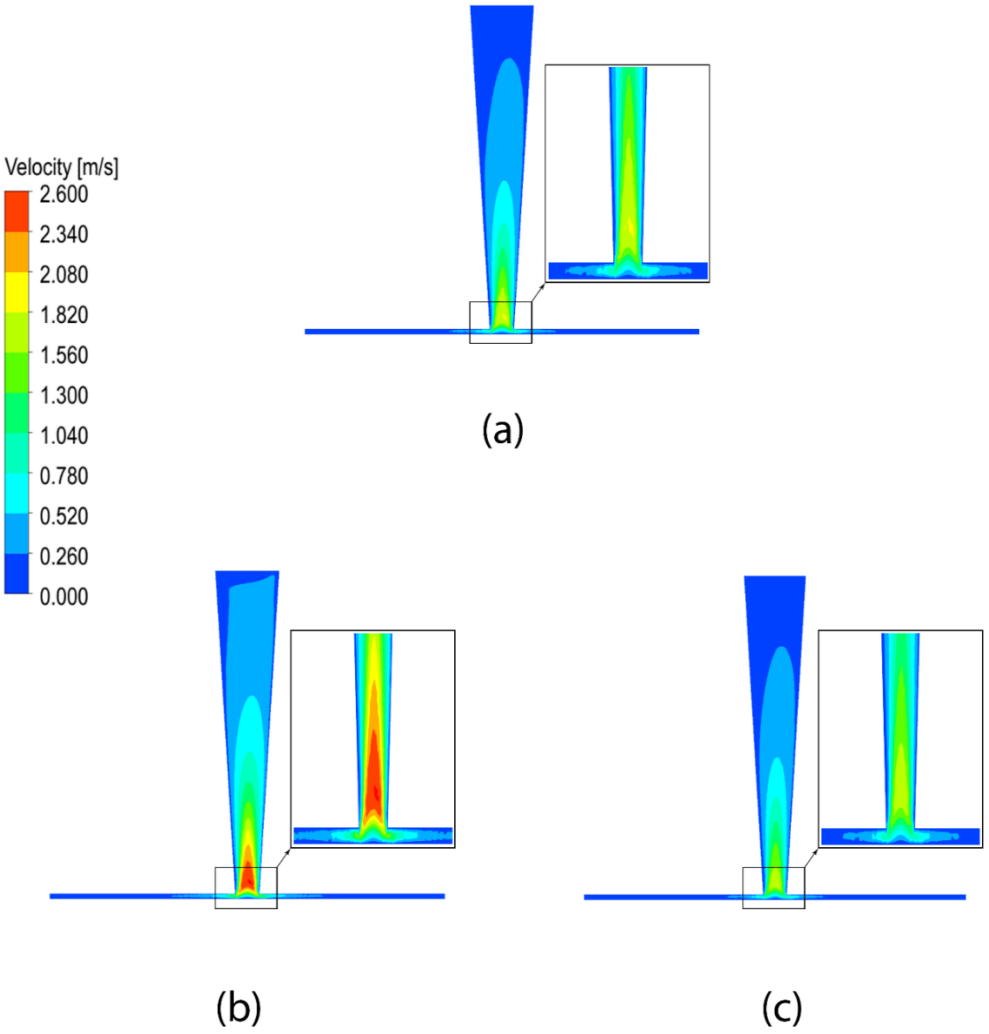

Figure 4.23: Simulation results for the air velocity distribution for case (a) at 7:30, case (b) at 11:30 and case (c) at 16:30 on 15 October 2018.

The air velocity increases inside the SCPP with an increase in the solar radiation intensity. The maximum air velocity occurred at 11:30 after which time it decreased gradually with the drop in irradiance (Figure 4.22). According to Figure 4.23, the irradiance had a positive effect and it is directly proportional to the amount of power;

therefore, the amount of solar radiation is an important factor in the improvement in performance and rise of output power.

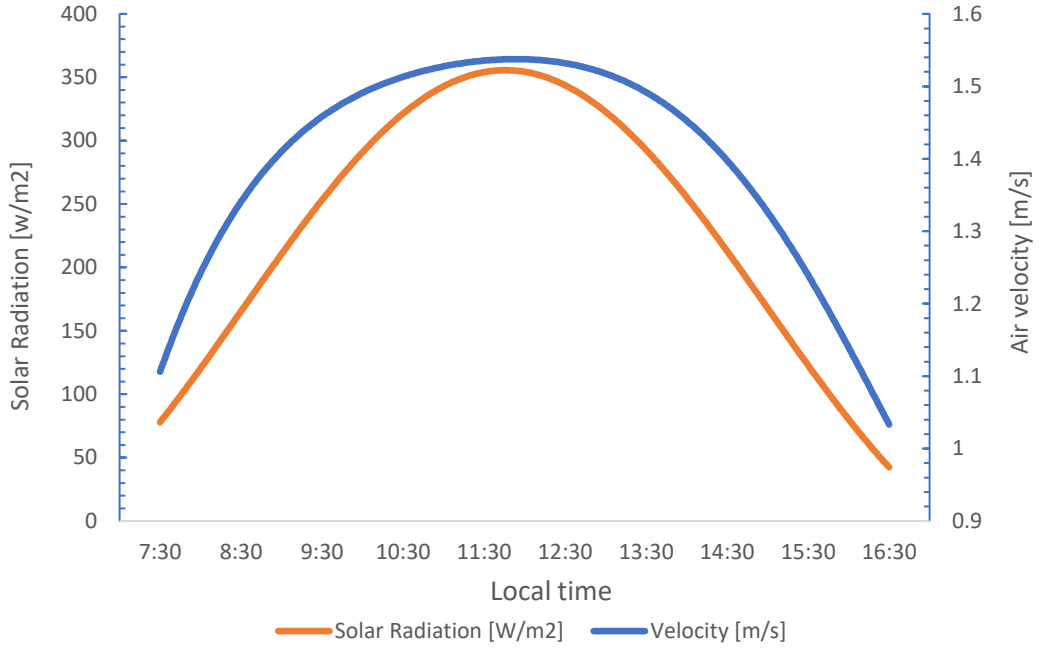

Figure 4.24: Variation of solar radiation with air velocity during the daytime on 15 October 2018.

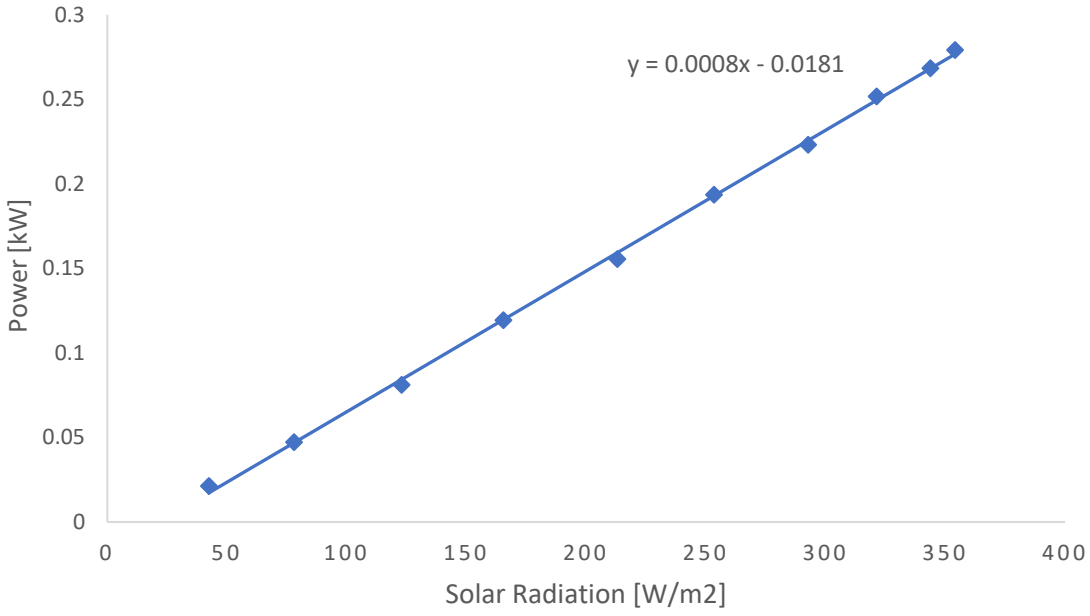

Figure 4.25 Variation of solar radiation with output power during the daytime on 15 October 2018.

Figure 4.26 illustrates the influence of solar radiation on static pressure variation. Case (b) has a good result because this hour has a higher amount of solar radiation than the other hours; therefore, it is clear to see the effects on the air velocity and thus the output power.

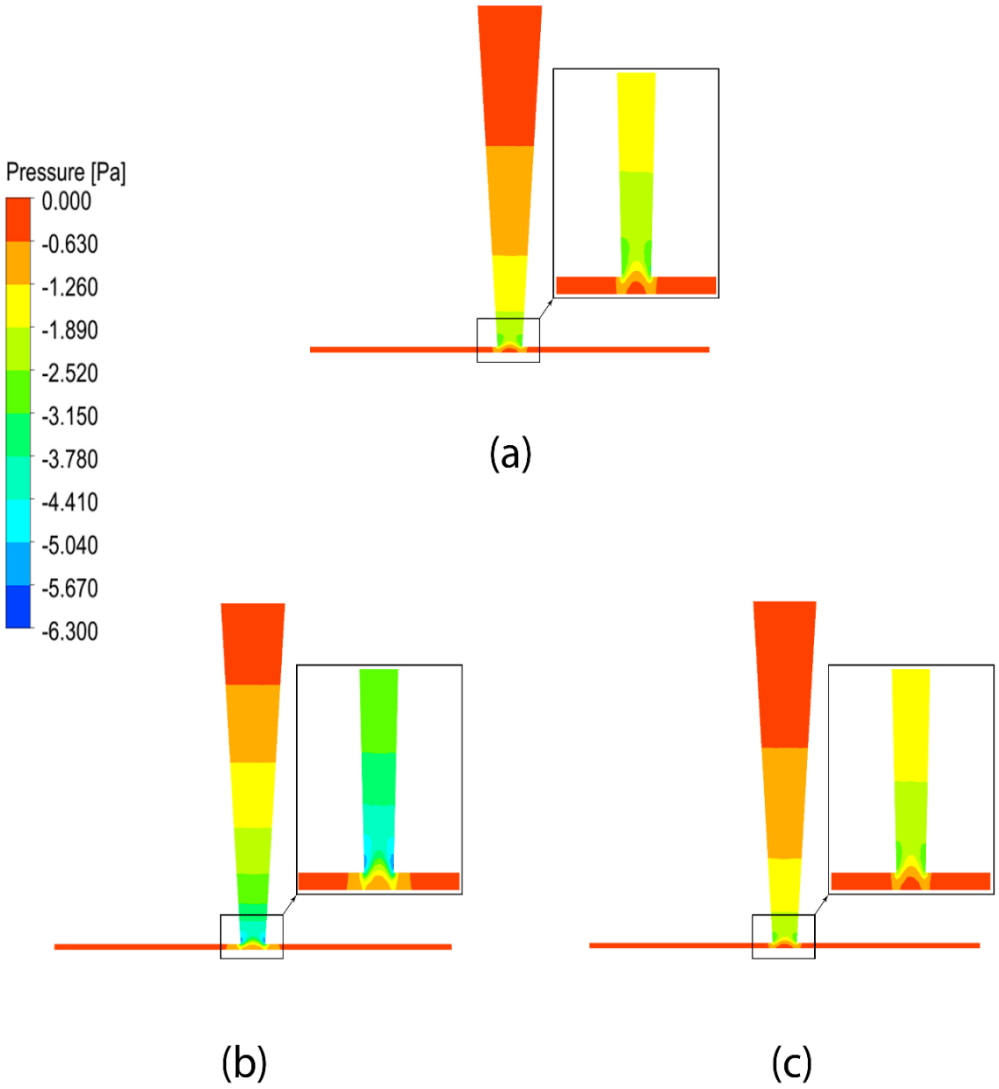

Figure 4.26: Simulation results of static pressure distribution for case (a at 7:30, case (b) at 11:30 and case (c) at 16:30 for 15 October 2018.

4.5 Comparison of Results between Seasons

The output power values differ between the months of the year as well as over hours of the same day. According to the results, the amount of solar irradiance has a direct effect on power generation capacity, as indicated in graphs 4.10, 4.15, 4.20, and 4.25.

Figure 4.27 shows output power versus time and as expected, the summer season exhibits great irradiance relative to the other seasons, so the airflow inside the SCPP increases leading to the rotation of the turbine blades and to power generation. Solar radiation increases with time beginning at sunrise and continuing until midday. In July, April, and January, the peak times are 12:30 pm; however, in October the peak time is 11:30 am after which time there is a gradual decrease until sunset.

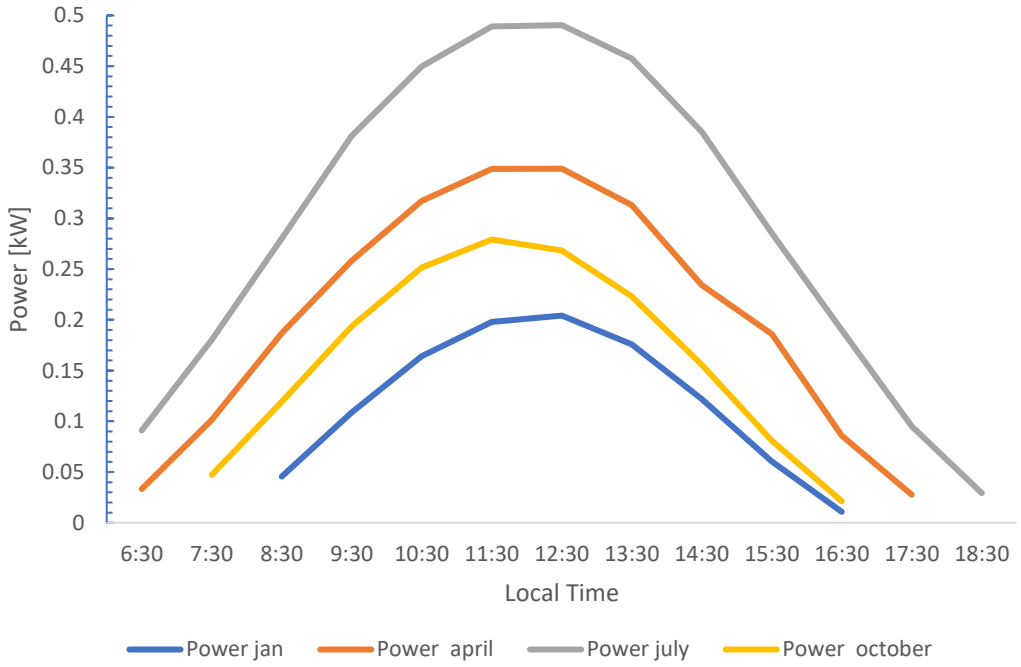

Figure 4.27: Output power rates for different seasons during the day.

In the Figure 4.28 the ambient temperature and monthly average global radiation is shown different months. The amount of solar radiation shows significant discrepancies between the months that lead to the power generation difference during the year.

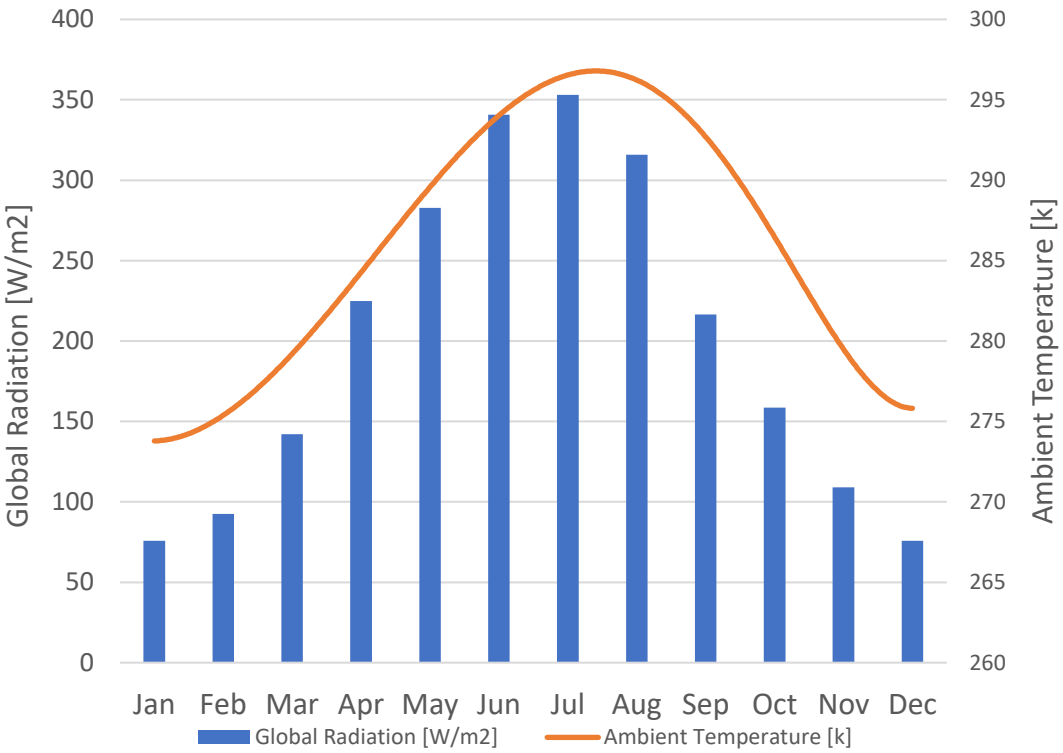

Figure 4.28: The ambient temperature and monthly average global radiation for Ankara between 2008-2009 [44]

CHAPTER 5

CONCLUSIONS AND FUTURE WORK

5.1 Conclusion

In recent decades, demand for energy has been significantly increased, and considering environmental impacts and the degrading nature of fossil fuels, clean and emission-free renewable energy production has attracted a great deal of attention. One of the most promising renewable energy sources is solar energy due to low cost and low harmful emissions, and from the 1980s, one of the most beneficial applications of solar energy is the utilization of solar chimney power plants (SCPP). An SCPP is a simple and reliable system that consists of three main components; a solar collector, a chimney and a tower to utilize electrical energy. Recently, by the advancement in computer technology, the use of CFD methodology for studying SCPP has become an extensive, robust and powerful technique. In light of the above, in this study, numerical simulations of an SCPP through two-dimensional axisymmetric modeling is performed. A numerical model is created using CFD software, and the results are verified with an experimental study from the literature. In the first part of the study, the optimum chimney geometry is finalized, which then will be used to design and construct the chimney prototype and compare the experimental results to study the performance parameters of the chimney, the wind turbine, electricity production, and coupling. As divergent chimney gives the best performance, selection of the chimney geometry is done considering this fact for further numerical and experimental studies, and inclination angle effect of the diverging chimney is studied for the performance of the solar chimney. According to the results, up to a critical inclination angle, increasing the angle rises the output power. About 3º of inclination angle, peak power is 2.18 times the benchmark case (case 1). After reaching peak power value, power decreases with increasing the inclination angle further. When divergence of the chimneys and effect of divergence angle on the performance are studied, it is found that divergence angle has a dominant effect on the SCPP performance. In this part, after obtaining the

best design for the solar chimney model with a 3.5-meter chimney height, 4-meter collector diameter, 0.06-meter collector height, 0.25-meter inlet chimney diameter, and a 0.6168-meter outlet chimney diameter, the amount of solar radiation and weather temperature were analyzed and the effects of the irradiance and air temperature on the output power of the SCPP were studied during the period. Ambient temperature is considered one of the factors that influences increasing collector efficiency in a negative or positive manner. The surrounding temperature and its influence on performance and power are analyzed and studied. Solar irradiance is considered to be the most important factor that impacts SCPP performance such that the absorber layer absorbs the irradiance that is lost through the natural convection. This helps to increase the value of heat into the solar chimney. The investigation includes the study of the relationship between solar insulation and ambient temperatures during the daytime. According to the results, power values are dependent on the amount of solar radiation as well as the ambient temperature.

5.2 Recommendations for the Future Work

For future works, our suggestion is performing the experimental studies based on a divergent chimney to calculate output power for each hour and comparing these results with the numerical results. Also turbine should be constructed and located to the middle part of the chimney in experimental studies. The effect of turbine blade geometry can be investigated as a further study.

REFERENCES

[1] International Journal Of Science and Research (IJSR) https://www.edfenergy.com/for-home/energywise/a-brief-history-of-energy (Access Date:07.01.2020)

[2] Solar Energy / description, Uses, & Facts / Britannica https://www.britannica.com/science/solar-energy (Access Date: 07.01.2020)

[3] The application study in solar energy teclonlogy for highway service; a case study of west lushan highway low carbon service area in china

[4] Outlook, E. (2010). International Energy Outlook. Outlook.

[5] Panwar, N. L., Kaushik, S. C., & Kothari, S. (2011). Role of renewable energy sources in environmental protection: A review. Renewable and Sustainable Energy Reviews, 15(3), 1513-1524.

[6] Kyoto Protocol – Wikipedia https://en.wikipedia.org/wiki/Kyoto_Protocol ((Access Date: 07.01.2020).

[7] Himri, Y., Malik, A. S., Stambouli, A. B., Himri, S., & Draoui, B. (2009). Review and use of the Algerian renewable energy for sustainable development. *Renewable and Sustainable Energy Reviews*, *13*(6-7), 1584-1591.

[8] Wagner, H. J. (2013). Introduction to wind energy systems. In EPJ Web of Conferences (Vol. 54, p. 01011). EDP Sciences.

[9] Kuriqi, A., Pinheiro, A. N., Sordo-Ward, A., & Garrote, L. (2019). Influence of hydrologically based environmental flow methods on flow alteration and energy production in a run-of-river hydropower plant. Journal of Cleaner Production.

[10] Gong, F., Guo, T., Sun, W., Li, Z., Yang, B., Chen, Y., & Qu, Z. (2019). Evaluation of geothermal energy extraction in Enhanced Geothermal System (EGS) with multiple fracturing horizontal wells (MFHW). Renewable Energy.

[11] Hanna, M. B., Mekhail, T. A. M., Dahab, O. M., Esmail, M. F. C., & Abdel-Rahman, A. R. (2016). Performance investigation of the solar chimney power plants heater case study in Aswan, Egypt. Journal of Power and Energy Engineering, 4(10), 39.

[12]https://www.bp.com/content/dam/bp/business sites/en/global/corporate/pdfs/energy-economics/statistical-review/bp-stats-review-2019-full-report.pdf](Access Date:07.01.2020)

[13]https://www.bp.com/content/dam/bp/business-sites/en/global/corporate/pdfs/energy-economics/statistical-review/bp-stats-review-2019-full-report.pdf](Access Date:07.01.2020)

[14] Kabir, E., Kumar, P., Kumar, S., Adelodun, A. A., & Kim, K. H. (2018). Solar energy: Potential and future prospects. Renewable and Sustainable Energy Reviews, 82, 894-900.

[15] Miller, G. T., & Spoolman, S. (2011). Living in the environment: principles, connections, and solutions. Nelson Education.

[16] Harish, P., Ramesh, K., Roshan, P.& Tarun, P. (2015). A sustainable approach for power generation: solar chimney, its application & theoretical considerations. International Journal of Research. 2(05)

[17] dos Santos Bernardes, M. A. (2010). Solar chimney power plants–developments and advancements. Solar Energy, 84(6), 978-953.

[18] Lorenzo, E. (2002). De Los Archivos Históricos De La Energía Solar Las chimeneas solares: De una propuesta española en 1903 a la Central de Manzanares. It reviews the history of the SUPPs technology.

[19] Papageorgiou, C. (2010). Floating solar chimney technology. Solar energy, 187-222.

[20] Günther, H. (1931). In hundred years-future energy supply of the world. *Stuttgart: Kosmos, Franckh'sche Verlagshandlung*.

[21] T. Hamilton, Mad Like Tesla: Underdog Inventors and Their Relentless Pursuit of Clean Energy. ECW Press, pp.93-103, 2011

[22] Von Backström, T. W., Harte, R., Höffer, R., Krätzig, W. B., Kröger, D. G., Niemann, H. J., & Van Zijl, G. P. A. G. (2008). State and recent advances in research and design of solar chimney power plant technology. *VGB powertech*, *88*(7), 64-71.

[23] Dhahri, A., & Omri, A. (2013). A review of solar chimney power generation technology. International Journal of Engineering and Advanced Technology, 2(3), 1-17.

[24] Ahmed, S. T., & Chaichan, M. T. (2011). A study of free convection in a solar chimney model. Engineering and Technology Journal, 29(14), 2986-2997.

[25]] Bouabidi, A., Ayadi, A., Nasraoui, H., Driss, Z., & Abid, M. S. (2018). Study of solar chimney in Tunisia: Effect of the chimney configurations on the local flow characteristics. Energy and Buildings, 169, 27-38.

[26] Osama, N. (2019). Numerical Study of the Effects of Geometric Parameters on Performance of Solar Chimney Power Plants. Master Thesis. Cankaya University, Ankara, Turkey

[27] Prototype Manzanares https://www.solar-updraft-tower.com/concept/prototype-manzanares/ (Access Date: 15.01.2020)

[28] Pasumarthi, N., & Sherif, S. A. (1998). Experimental and theoretical performance of a demonstration solar chimney model—Part I: mathematical model development. International Journal of Energy Research, 22(3), 277-288.

[29] Pasumarthi, N., & Sherif, S. A. (1998). Experimental and theoretical performance of a demonstration solar chimney model—Part II: experimental and theoretical results and economic analysis. International Journal of Energy Research, 22(5), 443-461.

[30] Zhou, X., Yang, J., Xiao, B., & Hou, G. (2007). Experimental study of temperature field in a solar chimney power setup. Applied Thermal Engineering, 27(11-12), 2044-2050.

[31] Atit Koonsrisuk, ―Analysis of flow in solar chimney for an optimal design purpose,‖ Thesis, Suranaree University of Technology, 2009.

[32] Koonsrisuk, A., & Chitsomboon, T. (2010, December). Theoretical turbine power yield in solar chimney power plants. In 2010 3rd International Conference on Thermal Issues in Emerging Technologies Theory and Applications (pp. 339-346). IEEE.

[33] Z. Ibrahim, etude et réalisation expérimentale du fonctionnement d'une tour solaire, Master thesis, Gafsa University-Tunisia, 2009.

[34] Al-Kayiem, H. H., & Aja, O. C. (2016). Historic and recent progress in solar chimney power plant enhancing technologies. Renewable and Sustainable Energy Reviews, 58, 1269-1292.

[35] Najmi, M., Nazari, A., Mansouri, H., & Zahedi, G. (2012). Feasibility study on optimization of a typical solar chimney power plant. Heat and Mass Transfer, 48(3), 475-485

[36] Ahmed, S. T., & Chaichan, M. T. (2011). A study of free convection in a solar chimney model. Engineering and Technology Journal, 29(14), 2986-2997.

[37] Hamilton, T. (2011). Mad Like Tesla: Underdog Inventors and Their Relentless Pursuit of Clean Energy. ECW Press.

[38] Maia, C. B., Ferreira, A. G., Valle, R. M., & Cortez, M. F. (2009). Theoretical evaluation of the influence of geometric parameters and materials on the behavior of the airflow in a solar chimney. Computers & Fluids, 38(3), 625-636.

[39] Bouabidi, A., Ayadi, A., Nasraoui, H., Driss, Z., & Abid, M. S. (2018). Study of solar chimney in Tunisia: Effect of the chimney configurations on the local flow characteristics. Energy and Buildings, 169, 27-38.

[40] Hu, S., Leung, D. Y., & Chan, J. C. (2017). Impact of the geometry of divergent chimneys on the power output of a solar chimney power plant. Energy, 120, 1-11.

[41] Larbi, S., Bouhdjar, A., & Chergui, T. (2010). Performance analysis of a solar chimney power plant in the southwestern region of Algeria. Renewable and Sustainable Energy Reviews, 14(1), 470-477.

[42] Sangi, R. (2012). Performance evaluation of solar chimney power plants in Iran. Renewable and Sustainable energy reviews, 16(1), 704-710.

[43] Bernardes, M. D. S., Voß, A., & Weinrebe, G. (2003). Thermal and technical analyses of solar chimneys. Solar Energy, 75(6), 511-524.

[44] Çağlar, A., Yamalı, C., Baker, D. K., & Kaftanoğlu, B. (2013). Measurement of solar radiation in Ankara, Turkey. Journal of Thermal Science and Technology, 33(2), 135-142

[45] El-Ghonemy, A. (2016). Solar chimney power plant with collector. IOSR Journal of Electronics and Communication Engineering (IOSR-JECE), 2, 28-35.

[46] Ayadi, A., Driss, Z., Bouabidi, A., & Abid, M. S. (2017). Experimental and numerical study of the impact of the collector roof inclination on the performance of a solar chimney power plant. Energy and Buildings, 139, 263-276.

[47] Patel, S. K., Prasad, D., & Ahmed, M. R. (2014). Computational studies on the effect of geometric parameters on the performance of a solar chimney power plant. Energy conversion and Management, 77, 424-431.

[48] Kasaeian, A. B., Heidari, E., & Vatan, S. N. (2011). Experimental investigation of climatic effects on the efficiency of a solar chimney pilot power plant. Renewable and Sustainable energy reviews, 15(9), 5202-5206.

[49] Al-Dabbas, A. M. (2011). A performance analysis of solar chimney thermal power systems. Thermal Science, 15(3), 619-642.

[50] Kulunk, H. (1985). A prototype solar convection chimney operated under Izmit conditions. In Proceedings of the 7th Miami international conference on alternative energy sources (Vol. 162).

[51] Najmi, M., Nazari, A., Mansouri, H., & Zahedi, G. (2012). Feasibility study on optimization of a typical solar chimney power plant. Heat and Mass Transfer, 48(3), 475-485.

[52] Zhou, X., Yang, J., Xiao, B., & Hou, G. (2007). Simulation of a pilot solar chimney thermal power generating equipment. Renewable Energy, 32(10), 1637-1644.

[53] BUĞUTEKİN, A. (2012). Experimental study of temperature field in a solar chimney plant in ADIYAMAN. Isi Bilimi ve Teknigi Dergisi/Journal of Thermal Science & Technology, 32(2).

[54] Hamdan, M. O., & Rabbata, O. (2012). Experimental solar chimney data with analytical model prediction. In Proceedings of the Solar Conference (Vol. 1, pp. 327-332).

[55] Kalash, S., Naimeh, W., & Ajib, S. (2013). Experimental investigation of the solar collector temperature field of a sloped solar updraft power plant prototype. Solar Energy, 98, 70-77.

[56] Dhahri, A., Omri, A., & Orfi, J. (2014). Numerical study of a solar chimney power plant. Research Journal of Applied sciences, engineering and Technology, 8(18), 1953-1965.

[57] Ferreira, A. G., Maia, C. B., Cortez, M. F., & Valle, R. M. (2008). Technical feasibility assessment of a solar chimney for food drying. Solar Energy, 82(3), 198-205.

[58] Ousmane, M., Dianda, B., Kam, S., Konfé, A., Ky, T., & Bathiebo, D. J. (2015). Experimental study in natural convection. Global journal of pure and applied sciences, 21(2), 155-169.

[59] Ghalamchi, M., Kasaeian, A., Ghalamchi, M., & Mirzahosseini, A. H. (2016). An experimental study on the thermal performance of a solar chimney with different dimensional parameters. Renewable Energy, 91, 477-483.

[60] Zhou, X., Yang, J., Xiao, B., Hou, G., & Xing, F. (2009). Analysis of chimney height for solar chimney power plant. Applied Thermal Engineering, 29(1), 178-185.

[61] Kalogirou, S. A. (2013). Solar energy engineering: processes and systems. Academic Press.

[62] Menter, F. R. (1994). Two-equation eddy-viscosity turbulence models for engineering applications. AIAA journal, 32(8), 1598-1605.

[63] Heat transfer - jack p. holman - Mcgraw-Hill education jan 13 2009 2017.

[64] Rao, J. S. (2017). Simulation based engineering in fluid flow design. Springer.

[65] FLUENT, ANSYS Fluent User Guide- FLUENT 18.2.

APPENDIX

Table A1: Solar radiation and ambient temperatures during the daytime for 17 January 2018.

Time	Total solar radiation (W/m^2)	Heat flux (W/m^2)	Ambient Temperature (K)
08:30	39.6	36	278.2
09:30	90.4	81.3	278.6
10:30	138.6	124.7	279
11:30	169.9	152.9	279.7
12:30	175	157.5	279.7
13:30	152.4	137.2	279.75
14:30	108.8	97.9	279.5
15:30	57.12	51.4	279.2
16:30	13	11.7	279.2

Table A2: Solar radiation and ambient temperature values during the daytime on 17 July 2018.

Time	Total heat solar radiation (W/m^2)	Heat flux (W/m^2)	Ambient Temperature (K)
06:30	132.3	119.1	293.5
07:30	241.3	217.1	296.3
08:30	359.1	323.2	297.8
09:30	470.4	423.3	298.2
10:30	558.5	502.6	299.3
11:30	609.3	548.4	299.8
12:30	614.6	553	300.7
13:30	573.2	515.9	301
14:30	492.3	443.1	301
15:30	384.7	346.3	300.3
16:30	266.9	240.2	299.9
17:30	154.9	139.4	299.2
18:30	61.3	55.1	298

Table A3: Solar radiation and ambient temperature values during the daytime on 15 October 2018.

Time	**Total heat solar radiation (W/m^2)**	**Heat flux (W/m^2)**	**Ambient Temperature (K)**
07:30	78	70.2	292.45
08:30	165.4	148.9	293.8
09:30	253.3	227.9	295.6
10:30	321.3	289.2	296.4
11:30	354.2	318.6	296.9
12:30	343.7	309.3	297.5
13:30	292.7	263.4	297.2
14:30	212.9	191.7	296
15:30	122.8	110.6	294.4
16:30	42.4	38.1	292

Table A4: Solar radiation and ambient temperature values during the daytime on 15 April 2018.

Time	Total heat solar radiation (W/m^2)	Heat flux (W/m^2)	Ambient Temperature (K)
06:30	53.4	48	288.5
07:30	128.9	116	289.6
08:30	217.1	195.3	290.6
09:30	303.6	273.2	291.5
10:30	372.8	335.5	292.9
11:30	411.5	370.4	294
12:30	412.2	371	294
13:30	374.7	337.2	294
14:30	306.3	2750.7	294
15:30	220.2	198.1	292.9
16:30	131.8	118.6	291.4
17:30	55.7	50	289.5